THE INFLUENCE OF CARBURISING TEMPERATURE ON THE CASE DEPTH AND PROPERTIES OF VACUUM CARBURISED PRECISION GEARS

by

Paul Johan Heintzberger

Submitted in partial fulfillment of the requirements for the degree

Master of Science (Applied Science): Metallurgy

in the Faculty of Engineering, the Built Environment and Information Technology,
University of Pretoria

September 2017

Acknowledgements

This has been both an exciting adventure as well as a tribulation. Without the support and guidance from a number of people this would not have been possible. My heartfelt thanks goes to:

1. Johannes and Frida Heintzberger, Dad and Mom – Thanks for all the wonderful years of “pushing” and love.
2. To Liesl, wife and mom, at last it is over. Thanks for all the support. The study may now be cleaned and the bonfire prepared.
3. Finally to Professor Madeleine Du Toit and Professor Pieter Pistorius, the alpha and omega, thanks for your tireless support and comments.

ABSTRACT

Low pressure gas carburising (LPGC) or vacuum carburising is a heat treatment process used in the aerospace and automotive industries to surface harden low alloy steel parts with carbon in the range of 0.1 to 0.25%. This project examined the LPGC process used to case harden precision gears and shafts used in various helicopter engines. Due to the stringent quality requirements specified by the OEMs (Original Engine Manufacturers) and by aerospace quality standards, approval can only be ensured through careful control of the carburising temperature, time and atmosphere during heat treatment. Final acceptance requires that the case depth, surface hardness, core hardness and component microstructure (related to the effectiveness of the quench and temper process) be controlled to within strict tolerances.

This investigation utilised an industrial vacuum carburising furnace and an acetylene atmosphere to examine the effect of carburising temperature on the properties of the carburised surface layer in parts machined from 16NCD13 carburising steel. The project aimed to determine whether the total carburising time could be decreased by increasing the carburising temperature without adversely affecting the specified case depth, hardness values or microstructure. The predictions of published carbon diffusion models (taking into account the influence of temperature, changing carbon concentration and alloying element content on the diffusion coefficient of carbon in austenite) were compared with the carbon concentration profiles measured after carburising at four different combinations of time and temperature.

The results showed that increasing the carburising temperature from 900° to 940°C, while reducing the carburising time from 104 to 64 minutes, did not have any detrimental effect on the case depth, case hardness, core hardness, component microstructure or part dimensions, while resulting in a significant reduction in the total carburising time. The mechanical properties of the test pieces were within specification and the grain size was not adversely affected by the higher heat treatment temperature. Increasing the carburising temperature to 960°C (and simultaneously reducing the carburising time to 44 minutes), however, caused a reduction in mechanical properties to below specification. Published carbon diffusivity models that consider the influence of temperature, increasing carbon concentration and the alloy content of the component were found to predict the actual carbon concentration profiles to a reasonable degree of accuracy.

TABLE OF CONTENTS

CHAPTER 1 – INTRODUCTION

Low pressure gas carburising (LPGC) (also referred to as vacuum carburising) is widely used in the aerospace and automotive industries as a surface hardening heat treatment. This project examined the LPGC heat treatment process used by Turbomeca Africa to surface harden precision gears and shafts used in various helicopter engines. The parts are profiled using CNC (computer numerical control) machines from low alloy carburising steel bar stock (up to 270 mm diameter). The bars are supplied in the annealed condition with a maximum permitted hardness of 240 BHN (hardness on the Brinell scale). Once machined to the desired tolerances, the parts are carburised, annealed and ground to the required final dimensions. After the final grinding step, the parts are hardened and tempered, followed by shot peening to generate compressive residual stresses on the surface of the component.

This investigation examines the feasibility of reducing the total carburising time of precision gears by increasing the carburising temperature in the furnace.

1.1 CARBURISING – AN OVERVIEW

Carburising is a thermochemical heat treatment process during which low carbon steel absorbs carbon liberated when the steel is heated in the presence of a carbon bearing compound or atmosphere, such as charcoal, cyanide salt or carbon monoxide. The aim of commercial carburising treatments is to increase the carbon content to sufficiently high levels that quenching produces a hard, wear-resistant martensitic case superimposed on a tough, low carbon steel core [1]. The carburising process is usually carried out at temperatures above the A_3 temperature (as shown in Figure 1.1 [2]) in the austenite phase field, where austenite is defined as an interstitial solid solution of carbon dissolved in γ-iron. Since the core material has a low carbon content, carbon atoms diffuse from the surface of the component into the core at the carburising temperature. The rate of carbon diffusion in austenite at a given temperature is dependent on the diffusion coefficient and the carbon concentration gradient [1].

At typical carburising temperatures (usually in the range of 800°C to 1050°C) austenite has a high solubility for carbon, with the maximum amount of carbon able to dissolve in austenite at the carburising temperature determined by the A_{cm} line on the Fe-Fe_3C phase diagram (Figure 1.1). The carbon content at the surface must be high enough to form a martensitic case with sufficient hardness to ensure high wear resistance after heat treatment. The required carbon content at the surface after diffusion is usually in the range of 0.8 percent to 1.0 percent. Higher surface carbon contents may result in excessive retained austenite levels or promote the formation of proeutectoid cementite networks at the grain boundaries, leading to flaking and premature failure in gears [1].

Since steel is carburised in the austenite phase field, direct quenching from the carburising temperature hardens both the case and the core if the cooling rate is greater than the critical cooling rate to form martensite. The steel can also be slow cooled after carburising, followed by austenitising and quenching as heat treatment steps separate from the carburising

operation. After quenching the steel is tempered at a low temperature to improve toughness and ductility without sacrificing hardness and wear resistance [1].

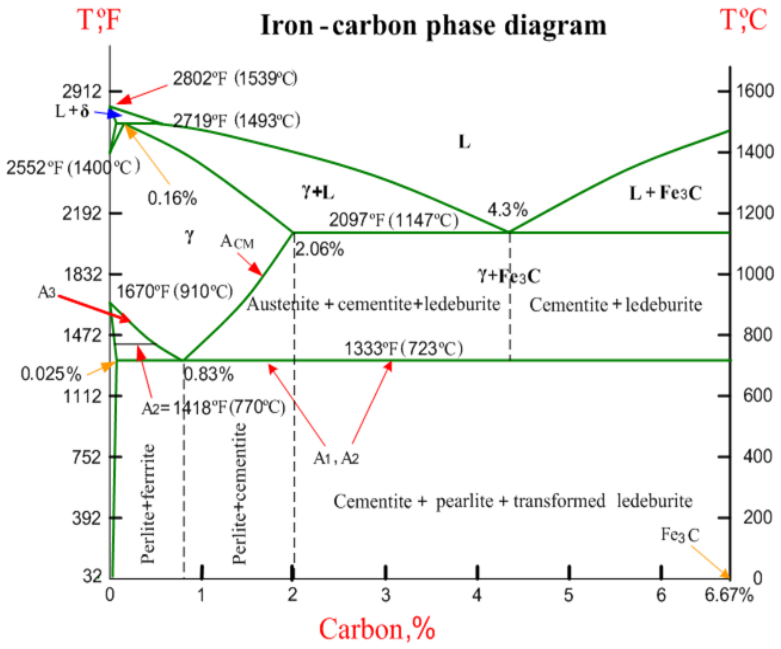

Figure 1.1. *The equilibrium Fe-Fe_3C binary phase diagram [2].*

1.2 CARBURISING METHODS

Commercial carburising may be accomplished by means of pack carburising, gas or vacuum carburising and liquid (salt bath) carburising. These processes are described below. Since this project is concerned with the vacuum carburising of precision gears, the discussion will focus on this process, with the remaining carburising processes included for information.

1.2.1 Pack carburising:

During pack carburising, the parts to be hardened are packed in a container with a solid carburising compound (such as cast iron shavings, hardwood charcoal or coke). The process is illustrated schematically in Figure 1.2. The container is closed and heated to a carburising temperature of around 900°C for the required amount of time and then slow cooled. At the carburising temperature, the carbonaceous compound reacts with air to form carbon monoxide, a strong reducing gas. The carbon monoxide decomposes into nascent carbon and carbon dioxide at the metal surface. Carbon diffuses into the steel surface to form the carburised layer, while the carbon dioxide gas immediately reacts with the carbonaceous material present in the solid carburising compound to produce fresh carbon monoxide (as shown by reaction (1.1)) [1,3].

The formation of carbon monoxide is enhanced by the addition of energisers or catalysts, such as barium carbonate ($BaCO_3$), calcium carbonate ($CaCO_3$), potassium carbonate (K_2CO_3) and sodium carbonate (Na_2CO_3), to the carburising compound. These carbonates promote the reduction of carbon dioxide with carbon to form carbon monoxide. Carburising continues as long as enough carbon is present to react with the excess carbon dioxide [1].

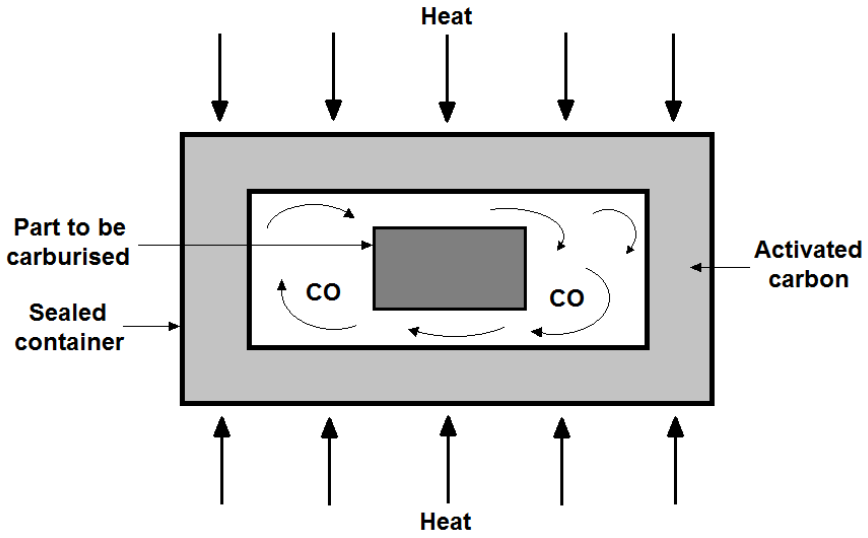

Figure 1.2. *Schematic illustration of the pack carburising process [4].*

$$CO_2\,(g) + \underline{C} \rightarrow 2CO\,(g) \qquad \ldots(1.1)$$

The surface carbon content obtained during pack carburising is typically in the range of 0.7 to 1.3%, depending on the process environment and carburising time. The typical case depths are approximately 0.1 to 1.5 mm, although case depths of more than 0.7 mm are preferred due to the variations in case depth inherent to the process. The principal advantages of pack carburising are that the process does not require the use of a prepared atmosphere and is efficient and economical for the processing of small batches or very large parts. It is, however, no longer a major commercial process although it is still used in a number of specialised applications. It is not well suited to the production of thin carburised cases that must be controlled to close tolerances and it cannot provide close control over surface carbon content as uniform temperatures are difficult to maintain. Parts cannot be quenched directly from the carburising temperature and heating and cooling of the charge is time consuming. Pack carburising has largely been replaced by the more readily controlled, more environmentally friendly and less labour intensive gas and vacuum carburising processes [1,3].

1.2.2 Liquid (salt bath) carburising:

Liquid carburising is the process of case hardening steel by placing the part in a bath of molten cyanide salt (typically consisting of sodium cyanide, sodium chloride and sodium carbonate in various concentrations) to allow carbon diffusion from the salt into the metal surface. Low temperature salt baths (best suited for case depths up to 0.75 mm) usually contain 20 percent cyanide and operate at temperatures between 845°C and 900°C. For case depths between 0.75 mm and 3.0 mm, high temperature salt baths operating at temperatures between 900°C and 950°C are preferred. Liquid carburising is best suited to small and medium-sized parts. Advantages include freedom from surface oxidation and soot formation, uniform case depth and carbon content, rapid rate of penetration and fast heating to temperature as a result of the high thermal conductivity of the salt bath. Cyanide salts are, however, toxic and corrosive and careful attention to safety is required [1,3].

1.2.3 Gas carburising:

During gas carburising low carbon steel is heated in an enriched furnace atmosphere containing carbon monoxide and/or hydrocarbon gas which readily decomposes at the carburising temperature. The component is held in a furnace in an atmosphere consisting of natural gas, methane or propane with a neutral carrier gas obtained from an endothermic generator, usually a mixture of N_2, CO, CO_2, H_2 and CH_4. The gas is continuously replenished and adjusted to maintain a constant carbon potential of approximately 0.8%. At the carburising temperature, the hydrocarbon gas decomposes at the component surface to form nascent carbon and hydrogen, with carbon diffusing into the surface. The carburising temperature is usually around 925°C and the carburising time ranges from 2 hours for a 1 mm depth case to a maximum of around 36 hours for a 4 mm case. Gas carburising can be performed as either a batch or continuous operation [1,3,5].

In addition to varying the carburising temperature, carburising time and composition of the furnace atmosphere, the surface carbon content can also be controlled by using a diffusion cycle, during which the gas flow in the furnace is interrupted at the carburising temperature. Carbon diffuses from the surface into the interior of the part, lowering the surface carbon content to prevent the formation of grain boundary cementite networks or retained austenite. The inclusion of a diffusion period also produces cleaner components as the carbon deposit (soot) that forms on the surface during carburising dissipates during the diffusion cycle. Gas carburising allows direct quenching from the carburising temperature, and ensures lower cost, cleaner surroundings, closer quality control and greater flexibility of operation compared to pack or liquid carburising. The quenching medium is usually oil, but can be water, brine or caustic soda depending on the component size and hardenability [1,3].

1.2.4 Vacuum carburising:

Vacuum carburising, also referred to as *low pressure gas carburising*, is performed by heating a low carbon steel component to the carburising temperature in rough vacuum, followed by a carbon boost cycle in a low pressure atmosphere containing hydrocarbon gas. After carburising, one or more diffusion cycles are performed at the carburising temperature (with interrupted gas supply), before the part is quenched in either oil or gas. Vacuum carburising is particularly effective for the case hardening of precision gears as parts carburised in vacuum and quenched in inert gas undergo less distortion than in more conventional carburising processes [1].

The use of low pressure vacuum carburising for aerospace applications has experienced tremendous growth in the last two decades as a result of reduced processing times and more environmentally-friendly technology. In 2010 it was estimated that the market share for vacuum carburising was between 10 and 15%, with expected growth reaching 30 to 40% in the years leading up to 2020 [6,7].

The use of acetylene gas as carbon source during vacuum carburising eliminates the soot and tar problems associated with vacuum carburising in other hydrocarbon atmospheres. The acetylene gas readily dissociates into carbon and hydrogen at the carburising temperature in accordance with reaction (1.2) [1,3,5].

$$C_2H_2\ (g) \rightarrow 2\underline{C} + H_2\ (g) \qquad \ldots(1.2)$$

The dissociated carbon is absorbed by the steel surface, rapidly increasing the surface carbon concentration up to the maximum carbon solubility in austenite at the carburising temperature. Vacuum carburising with acetylene is a diffusion-controlled process as the dissociation of acetylene in the furnace atmosphere and the adsorption of nascent carbon at the steel surface occur much faster than carbon diffusion into the steel [8]. The importance of diffusion during carburising is considered in more detail in Chapter 2.

Vacuum carburisation with acetylene gas has a number of advantages over conventional gas carburisation [9,10]:

- Intergranular surface oxidation is prevented, which eliminates initial wear on the surface, enhances resistance to microcracking and improves fatigue performance.
- Vacuum treatment ensures excellent surface finish and part cleanliness after carburising and heat treatment. The need for post-treatment cleaning is almost completely eliminated.
- The use of high pressure gas quenching from the carburising temperature reduces part distortion and minimises the amount of grinding and machining required after heat treatment to achieve set tolerances.
- The vacuum carburising process is characterised by excellent uniformity and repeatability, even for complex geometries and high load densities in the furnace. Narrow tolerances can be maintained and once the correct hardness profile has been achieved, it can be reproduced accurately.
- The need for endothermic gas generators is eliminated and process gas consumption is significantly reduced.
- Higher carburising temperatures can be used, decreasing processing times.
- Vacuum carburising is associated with high carbon availability at the steel surface and quick saturation of carbon in the surface layers.

Acetylene decomposition during vacuum carburising occurs under non-equilibrium conditions and conventional methods of furnace control therefore cannot be utilised. Computer simulations designed to predict the process parameters needed to achieve the desired case depths and carbon concentration profiles are used for process control. Other potential disadvantages of the process include [9]:

- Higher initial equipment costs.
- Vacuum carburising with high pressure gas quenching is not suitable for treating steels with low hardenability.
- Depletion of manganese at the surface of parts due to evaporation in the vacuum environment necessitates the use of low manganese steels alloyed with various other alloying elements to increase the hardenability to the required levels.
- Since acetylene gas is unstable at higher pressures, storage and supply costs are higher than for more conventional propane gas.

1.3 CARBURISING GASES

Various hydrocarbon gases can be used as carburising media during gas and vacuum carburising. These include methane, propane, ethylene and acetylene, all of which decompose at temperatures above 800°C [11].

Propane and methane are widely used in gas carburising applications. These hydrocarbon gases are premixed with air and react endothermically in a high temperature catalyst-filled generator. The carbon potential of the endothermic carrier gas produced by the generator is usually limited to a maximum of 0.6% to prevent sooting. A small amount of hydrocarbon gas can be introduced into the carrier gas should a higher atmospheric carbon potential be required, but the furnace atmosphere carbon potential seldom exceeds 1.2% [11].

The decomposition of most hydrocarbon gases is endothermic. As shown in reactions (1.3) to (1.5), saturated hydrocarbon gas, such as propane, requires several decomposition steps to reach an equilibrium state [12].

$$C_3H_8\,(g) \rightarrow \underline{C} + C_2H_6\,(g) + H_2\,(g) - 24.3\ kJ \quad \ldots(1.3)$$

$$C_2H_6\,(g) \rightarrow \underline{C} + CH_4\,(g) + H_2\,(g) - 23.0\ kJ \quad \ldots(1.4)$$

$$CH_4\,(g) \rightarrow \underline{C} + 2H_2\,(g) - 79.9\ kJ \quad \ldots(1.5)$$

The decomposition of saturated hydrocarbon gas, especially methane (CH_4), is generally slow. Acetylene is, however, an unsaturated hydrocarbon gas that readily decomposes exothermically, as shown in reaction (1.6) [12].

$$C_2H_2\,(g) \rightarrow 2\underline{C} + H_2\,(g) + 223.8\ kJ \quad \ldots(1.6)$$

The decomposition of acetylene is several times faster than that of propane and the risk of sooting is reduced [13]. The use of acetylene during gas carburising is associated with high carbon availability [14]. Each acetylene molecule decomposes into two free carbon atoms and one hydrogen molecule, with no intermediate carbon chain such as methane formed. The amount of carbon delivered by each acetylene molecule is therefore double that of most other hydrocarbons used in carburising applications, ensuring more efficient transfer. The hydrogen formed on decomposition of the acetylene reduces the steel surface, ensuring a cleaner component and more effective transfer of carbon from the atmosphere.

Since vacuum carburising in an acetylene environment is a diffusion-controlled process, the influence of diffusion on the vacuum carburisation process is described in more detail in Chapter 2.

CHAPTER 2 – LITERATURE SURVEY

Carburisation is a surface hardening treatment that relies on diffusion to facilitate the migration of carbon atoms into the surface layers of a low carbon steel substrate. A carbon concentration gradient is produced in the part, with the highest carbon content at the surface of the component. During gas carburising the surface carbon concentration achieved is determined by the composition of the gas atmosphere, the carburising temperature, the carburising time and the solubility of carbon in the steel [1].

In order to understand the influence of temperature on the gas carburisation process, a thorough understanding of the nature of diffusion in metals is required. This chapter describes the mechanisms of diffusion in metallic materials and examines the predictive models that have been proposed to describe the influence of diffusion on carburisation. The effect of a proposed increase in carburisation temperature on the total carburisation time and the steel grain size is also considered.

2.1 SOLID-STATE DIFFUSION MECHANISMS

Solid-state diffusion is defined as the migration of individual atoms (or ions) through the lattice of crystalline structures and other solid non-metallic materials [15]. The laws governing atomic diffusion were first proposed by Adolf Fick in 1855 [16] and are considered in more detail in §2.2 and §2.3. Diffusion is considered to be statistical in nature, resulting from random movements of individual atoms. While the migration of an individual atom may be random and unpredictable, the movement of large numbers of atoms in a structure tends to be more systematic [15].

Two distinct diffusion mechanisms are observed in solid materials, namely vacancy diffusion and interstitial diffusion. Since carbon dissolves interstitially in iron, the interstitial diffusion mechanism, described in §2.1.2, is more relevant to the carburisation process.

2.1.1 Vacancy (substitutional) diffusion:

As shown in Figure 2.1, the vacancy diffusion mechanism involves the movement of substitutionally dissolved solutes (atoms) into adjacent vacant lattice sites. Diffusion occurs when the diffusing atom has enough energy to leave its equilibrium lattice position and jump into a neighbouring vacant site. A vacancy can typically exchange positions with any one of eight neighbours in a body centred cubic (BCC) crystal structure, or with twelve neighbouring atoms in a face centred cubic (FCC) material. The rate at which vacancy diffusion occurs is dependent on the number of vacancies in the crystal structure, as well as the activation energy required to carry out the exchange [15].

For an atom to move into an adjacent vacant site, it must overcome the energy barrier required for it to migrate past the atoms bordering the vacancy in order to reach the next equilibrium position in the lattice. This energy is usually supplied in the form of heat. With an increase in temperature, the amplitude of vibration of atoms around their equilibrium lattice positions increases, and the jump rate of these atoms into neighbouring vacancies rises [15].

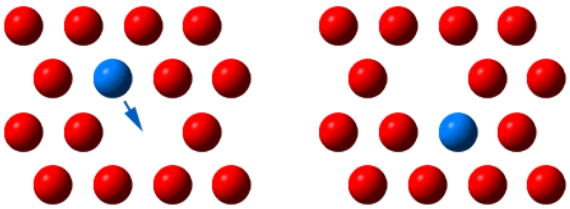

Figure 2.1. *Schematic illustration of the vacancy (substitutional) diffusion mechanism in crystalline materials [17].*

The number of vacancies in the crystal lattice also increases with an increase in temperature. As shown by equation (2.1), the number of vacancies (N_v) in a metallic crystal structure is strongly dependent on temperature [18].

$$N_v = N \exp(-E_v/kT) \quad \ldots(2.1)$$

where N is the total number of lattice sites, E_v is the energy required to form a vacancy, k is Boltzmann's constant (1.38×10^{-23} J.K^{-1} or 8.62×10^{-5} eV.K^{-1}) and T is temperature (K).

As temperature increases, the vacancy diffusion rate therefore increases as more activation energy becomes available, more vacancies are created and the atom jump rate increases.

2.1.2 Interstitial diffusion:

The interstitial diffusion mechanism, shown schematically in Figure 2.2, involves the movement of atoms from one interstitial site to another in the crystal structure. Interstitial atoms tend to be considerably smaller in diameter than the surrounding solvent atoms. Although more interstitial vacancies are usually available in the crystal lattice due to the low solubility of interstitial elements, movement of interstitially dissolved atoms requires considerable lattice distortion. Displacement of the lattice comprises the bulk of the activation energy barrier required for interstitial diffusion [15].

Carbon has a small atomic radius (0.67 Å) compared to that of the solvent iron atoms (1.56 Å) in the steel crystal structure. Carbon atoms therefore dissolve interstitially in iron, limiting the solid solubility [15]. As shown in Figure 1.1, the maximum solubility of carbon in γ-iron (FCC austenite) is approximately 2.0 percent at 1147°C, while the maximum solubility of carbon in α-iron (BCC ferrite) is only 0.025 percent at 723°C.

An increase in temperature accelerates interstitial diffusion by supplying the activation energy needed for atom migration and by increasing the jump frequency of the interstitially dissolved atoms.

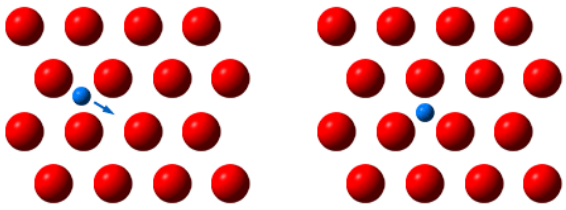

Figure 2.2. *Schematic illustration of the interstitial diffusion mechanism [17].*

2.1.3 Activation energy:

Activation energy is best described as the minimum energy required for a reaction to occur. To jump from one lattice site to another, an atom needs enough thermal energy to break the bonds between the neighbouring atoms and to facilitate the necessary lattice distortion during movement from one site to another. This energy is known as the activation energy for diffusion and is schematically illustrated in Figure 2.3 for the diffusion of an interstitially dissolved atom [15].

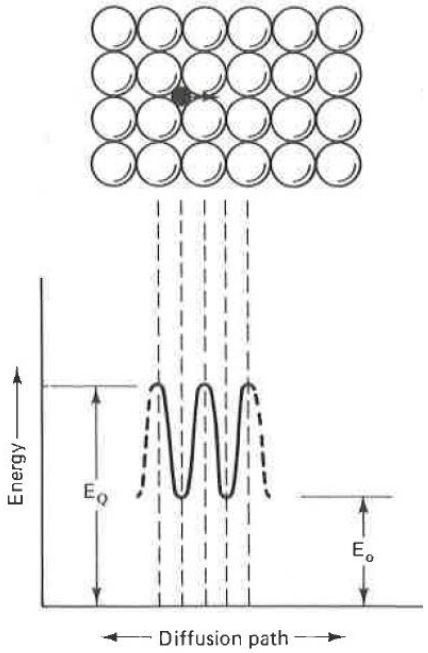

Figure 2.3. *Interstitial diffusion and the activation energy associated with the process (E_0 is the energy associated with the equilibrium lattice position; and E_Q is the energy barrier or activation energy [15].*

As described earlier, diffusion is a temperature-dependent process, with the diffusion rate increasing with an increase in temperature. An Arrhenius-type equation, shown in equation (2.2), can be used to describe the relationship between diffusion rate and temperature [15].

$$\text{Diffusion rate} = A \exp(-Q/RT) \quad \ldots(2.2)$$

where A is a constant (independent of temperature), Q is the activation energy for the process (J/mol), R is the universal gas constant (8.314 $J.mol^{-1}.K^{-1}$) and T is temperature (K).

If equation (2.2) is applied to the movement of an atom into a neighbouring vacancy, the number of jumps the atom makes per second can be estimated using equation (2.3). The jump rate increases significantly with an increase in temperature, emphasising the importance of temperature in determining the diffusion rate [15].

$$r_v = A \exp(-Q_m/RT) \quad \ldots(2.3)$$

where r_v is the jump rate (or the number of times per second an atom and a vacancy exchange positions), and Q_m is the activation energy for the movement of the atom.

2.2 FICK'S 1ST LAW OF DIFFUSION (STEADY-STATE DIFFUSION)

Fick's first law of diffusion is usually applied to steady-state diffusion, which implies that the diffusion flux and concentration gradient do not change with time. Diffusion takes place as a result of a concentration gradient which produces the driving force for atoms to migrate from regions of high concentration to regions of low concentration (illustrated schematically in Figure 2.4). Fick's First Law relates this concentration gradient to the flux, *J*, of atoms in the crystal matrix (that is the number of atoms passing through unit area in unit time) [15].

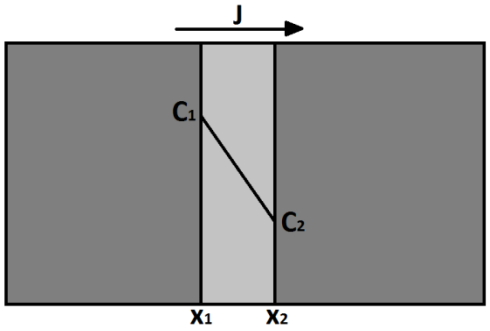

Figure 2.4. *Schematic illustration of the diffusion flux described by Fick's First Law.*

The basic expression for the dependence of the diffusion flux on concentration gradient is given by Fick's First Law, shown in equation (2.4) [15].

$$J = -D.\left(\frac{\delta C}{\delta x}\right) \qquad \ldots(2.4)$$

where *J* is the flux or net flow of atoms (atoms.m^{-2}.s^{-1} or kg.m^{-2}.s^{-1}), *D* is the diffusivity or diffusion coefficient (m^2.s^{-1}), *C* is the solute concentration and *x* is the diffusion distance (m). The derivative (δ*C*/δ*x*) is the concentration gradient (atoms.cm^{-3}.cm^{-1}).

If the diffusion process is linear, equation (2.5) applies (with reference to Figure 2.4).

$$\frac{\delta C}{\delta x} \sim \frac{\Delta C}{\Delta x} = \frac{C_2 - C_1}{x_2 - x_1} \qquad \ldots(2.5)$$

The flux of diffusing atoms, *J*, can be used to quantify the rate of diffusion and is defined as either the number of atoms diffusing through unit area per unit time (atoms.m^{-2}.s^{-1}), or as the mass flux, i.e. the mass of atoms diffusing through unit area per unit time (kg.m^{-2}.s^{-1}). The negative sign in equation (2.4) indicates that the atoms move from a region with a higher concentration to a region with a lower concentration [15].

The diffusion coefficient or diffusivity, *D*, in the diffusion equation is influenced by the nature of the diffusing species and the matrix through which the atoms diffuse, the bond strength and the crystal structure. The diffusion coefficient is also strongly temperature dependent. This temperature dependence is described by an Arrhenius-type equation, shown in equation (2.6) [15].

$$D = D_o \exp(-Q/RT) \qquad \ldots(2.6)$$

where D_o is the frequency factor (m^2.s^{-1}), *Q* is the activation energy (J.mol^{-1}), *T* is temperature (K) and *R* is the universal gas constant (8.314 J.mol^{-1}.K^{-1}).

This Arrhenius equation can be rewritten in the form of the straight line relationship shown in equation (2.7), which enables determination of the frequency factor and activation energy from experimental diffusion data.

$$\ln D = \ln D_o - \frac{Q}{RT} \quad \text{or} \quad \log D = \log D_o - \frac{Q}{2.3RT} \qquad \ldots(2.7)$$

Table 2.1 contains the diffusion data for carbon in iron that is relevant to the carburisation of steel [19]. Since carburisation usually takes place at temperatures within the FCC austenite phase field, the diffusion data for carbon in γ-iron is more relevant to this investigation. Since the FCC unit cell is more densely packed than the BCC unit cell, higher activation energy is required for the diffusion of carbon through austenite (γ) and the diffusion rate is lower in austenite than in ferrite (α) at the same temperature.

Table 2.1. *Diffusion data for carbon in α-iron and γ-iron [19].*

Diffusing element	*Diffusing through*	D_o *($m^2.s^{-1}$)*	*Q ($kJ.mol^{-1}$)*	*D ($m^2.s^{-1}$) at 900°C*
Carbon	α-iron	6.2×10^{-7}	80	1.7×10^{-10}
Carbon	γ-iron	2.3×10^{-7}	148	5.9×10^{-12}

2.3 FICK'S 2ND LAW OF DIFFUSION (NON-STEADY-STATE DIFFUSION)

Fick's Second Law describes non-steady-state diffusion and takes into account changes in concentration profile with time (as shown schematically in Figure 2.5). This situation most closely resembles carburisation during which the carbon concentration gradient changes as carbon is absorbed from the atmosphere and diffuses into the surface layers of the part. As shown in equation (2.8), Fick's Second Law is a second order differential equation which indicates that the rate of concentration change is proportional to the rate of change of the concentration gradient [15].

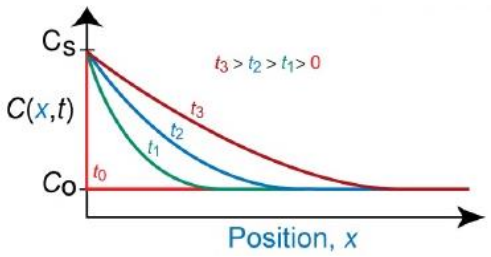

Figure 2.5. *Schematic illustration of the change in concentration gradient with time described by Fick's Second Law (adapted from [20]).*

$$\left(\frac{\delta C}{\delta t}\right) = D\left(\frac{\delta^2 C}{\delta x^2}\right) \qquad \ldots(2.8)$$

If the carbon concentration at the surface increases from an initial concentration of C_o to a concentration of C_S, Fick's Second Law assumes the form shown in equation (2.9) [15].

$$C_x - C_0 = (C_S - C_0)\left[1 - \text{erf}\left\{\frac{x}{(2\sqrt{(Dt)}}\right\}\right] \qquad \ldots(2.9)$$

where C_x is the required carbon concentration at a depth x below the surface.

Equation (2.9) can be modified to equation (2.10), known as the Van Ostrand-Dewey solution to Fick's Second Law. This equation is widely applied in carburising situations to calculate the carbon concentration as a function of depth below the surface.

$$\frac{C_S - C_x}{C_S - C_0} = \text{erf}\left(\frac{x}{2\sqrt{(Dt)}}\right) \quad \ldots(2.10)$$

where C_0 is the initial carbon content of the steel, C_S is the carbon concentration at the surface of the steel, C_x is the carbon concentration at a depth x below the surface, D is the carbon diffusion coefficient at the carburising temperature, and t is the carburising time in seconds.

The Gauss error function (erf) in equations (2.9) and (2.10) is defined by equation (2.11). A number of calculated erf (x) solutions for various values of x are shown in Table 2.2 [21].

$$\text{erf}\ (x) = \frac{2}{\sqrt{\pi}} \int_0^x \exp\ (-t^2)\, dt \quad \ldots(2.11)$$

Table 2.2. *Solutions to the error function equation for different values of x [21].*

x	*erf (x)*	*x*	*erf (x)*
0.00	0.0000000	0.50	0.5204999
0.05	0.0563720	0.55	0.5633234
0.10	0.1124629	0.60	0.6038561
0.15	0.1679960	0.65	0.6420293
0.20	0.2227026	0.70	0.6778012
0.25	0.2763264	0.75	0.7111556
0.30	0.3286268	0.80	0.7421010
0.35	0.3793821	0.85	0.7706681
0.40	0.4283924	0.90	0.7969082
0.45	0.4754817	0.95	0.8208908

The Van Ostrand-Dewey solution to the second order diffusion equation, shown in equation (2.10), offers an approximate solution to Fick's Second Law that is often applied to carburisation processes. This solution is, however, based on simplifying assumptions and three major complications should be noted:

- The diffusion coefficient, D, is not only a function of temperature, but also of concentration. Wells and Mehl [22] and Karabelchtchikova [23] confirmed that the diffusion coefficient of carbon in austenite increases with carbon content during carburisation. Actual carbon concentration profiles therefore differ from those calculated using Fick's Second Law, implying that carbon diffusivity models for carburisation applications should take into consideration the effect of changes in temperature as well as carbon concentration [24].

- In many carburisation treatments the temperature and surface carbon concentration may vary with time. After an initial period of carburisation, the surface carbon content and the temperature are usually lowered as part of a diffusion step (or multiple diffusion steps). This treatment allows the diffusion of carbon from the surface layers into the interior of

the component. This ensures that maximum hardenability is obtained at the steel surface after hardening and quenching, and minimises the risk of forming cementite networks [24].

- Alloying elements in the steel (such as manganese, chromium, silicon, nickel and molybdenum) may have a significant influence on carbon diffusion during the carburisation process. The effect of alloying elements on the carbon diffusion coefficient therefore needs to be taken into account when carbon concentration gradients are calculated [24].

This discussion indicates that carbon diffusivity models for predicting concentration profiles during carburisation should take into consideration the alloy content of the steel, as well as changes in temperature and carbon concentration during the carburisation cycle.

2.4 CARBON DIFFUSIVITY MODELS

In the early 1970s a mathematical model for predicting carbon concentration profiles in gas carburised steels was proposed by Collin *et al.* [25]. This model takes into account the carburising temperature, alloy composition of the steel and the changing carbon content of the part. The proposed formula for the carbon diffusion coefficient is given in equation (2.12). More recently Liu *et al.* [11] applied the equation developed by Collin *et al*. to determine the diffusion coefficient of carbon during vacuum carburising in an acetylene environment and reported good correspondence between calculated and measured carbon concentration profiles.

$$D = \frac{1.43\exp\left(-\frac{19700}{T}\right)\exp\left[0.00242\exp\left(\frac{6790}{T}\right)(\%\mathrm{C})\right]}{1-0.232(\%\mathrm{C})} \quad \ldots(2.12)$$

where T is the absolute temperature (K).

Equation (2.12) indicates that the diffusion coefficient for carbon in austenite, D, is a function of the carburising temperature and the carbon content of the steel. Wada *et al.* [26], however, pointed out that the diffusion coefficient of carbon is also influenced by the presence of alloying elements in the steel. Neumann and Person [27] suggested that the activity of carbon in the steel, a_c, should be adjusted by a factor q, which can be calculated by means of equation (2.13). The effect of alloying elements on the carbon diffusion coefficient can be incorporated into the Collin diffusion model by multiplying equation (2.12) with the value of q for a specific steel composition.

$$q = 1 + [\%Si](0.15 + 0.033[\%Si]) + 0.0365[\%Mn] - [\%Cr](0.13 - 0.0055[\%Cr]) + [\%Ni](0.03 + 0.00365[\%Ni]) - [\%Mo](0.025 + 0.01[\%Mo]) - [\%Al](0.03 + 0.02[\%Al]) - [\%Cu](0.016 + 0.0014[\%Cu]) - [\%V](0.22 - 0.01[\%V]) \quad \ldots(2.13)$$

where the element concentrations are given in percentage by mass.

Under the same carburising conditions, the carbon activity increases as the parameter q decreases. Conversely, the smaller the value of q, the lower the carbon potential needed to maintain constant carbon activity in the atmosphere. As a consequence, the q value can be used as an index for estimating the carburising performance of steels in a vacuum furnace.

Goldstein and Moren [24] subsequently modelled the vacuum carburisation process based on the assumption that the treatment consists of two steps: carburisation with a specific amount of gas backfilled into the furnace chamber, followed by diffusion to redistribute the initial carburisation profile. The authors reported good agreement between measured carbon concentration profiles and carbon contents calculated by means of equation (2.14).

$$D = \left(0.07 + 0.06(\%C)\right) \exp\left(-\frac{32000}{RT}\right) \quad \ldots(2.14)$$

where R is the universal gas constant (1.99 cal.mol^{-1}.K^{-1}).

In 1980 Tibbetts [28] investigated the diffusivity of carbon in iron and steel at temperatures between 975°C and 1075°C and developed an empirical relationship for the diffusion coefficient of carbon in austenite, shown in equation (2.15).

$$D = 0.47 \exp\left(-1.6\%\mathrm{C}\right) \exp\left(-\frac{37000-6600\%\mathrm{C}}{RT}\right) \quad \ldots(2.15)$$

where the parameter q can be calculated from equation (2.13) and R is the universal gas constant (1.99 cal.mol^{-1}.K^{-1}).

More recently, Jung *et al.* [10] calculated the Tibbetts carbon diffusivity using equation (2.16). The authors compared measured carbon concentration profiles with those calculated using the models proposed by Goldstein and Moren [24], Collin *et al.* [25] and Tibbetts [28], and reported good agreement with the measured results (as shown in Figure 2.6). It was reported that the carbon concentration profile calculated using the Collin formula, equation (2.12), showed the best agreement with the measured profile. This can be attributed in part to the fact that Collin calculated diffusivities at temperatures similar to those used in vacuum furnaces.

$$D = 0.47 \exp\left(-1.6\%\mathrm{C}\right) \exp\left(-\frac{154.9-27.63\%\mathrm{C}}{RT}\right) q \quad \ldots(2.16)$$

where the parameter q can be calculated from equation (2.13) and R is the universal gas constant (8.314 J.mol^{-1}.K^{-1}).

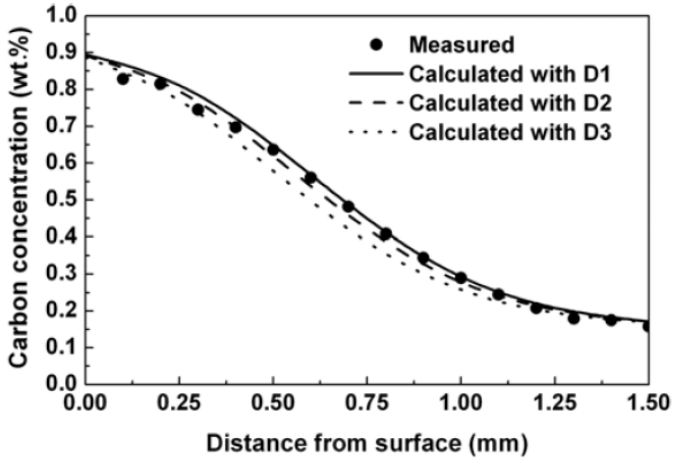

Figure 2.6. *Comparison of the carbon concentration profiles calculated using different carbon diffusivities in the Fe-C binary system. D1, D2, and D3 refer to the carbon diffusivities proposed by Tibbetts [28], Collin et al. [25] and Goldstein and Moren [24], respectively [10].*

2.5 CARBURISING TIME

The preceding discussion showed that the diffusion rate of carbon in austenite increases with an increase in the carburising temperature. This suggests that the total carburising time can be decreased by increasing the carburisation temperature.

The final case depth after carburising can be calculated as a function of time using the Einstein equation, shown in equation (2.17) [29]. This allows calculation of the required carburisation time to achieve a constant case depth if the carburisation temperature is increased.

$$x = 1{,}414\sqrt{Dt} \quad \ldots(2.17)$$

where x is the case depth, t is the time in hours at temperature, and D is the diffusion coefficient.

The case depth (mm) can also be calculated from equation (2.18) [30].

$$x = \frac{0.79(Dt)^{1/2}}{0.24+\frac{C_{x,t}-C_S}{C_S-C_0}-0.7\frac{D}{\beta}} \quad \ldots(2.18)$$

where x is the case depth (cm), D is the carbon diffusion coefficient in austenite ($cm^2.s^{-1}$), t is the carburising time (s), $C_{x,t}$ is the carbon content at case depth x after carburising time t, C_0 is the initial carbon content of the steel, C_S is the surface carbon content after carburising, and β is the carbon transport coefficient from the atmosphere to the steel surface ($cm.s^{-1}$).

It is evident that increasing the carburising temperature reduces the required carburising time to achieve a specified case depth by increasing the carbon diffusion rate, but it should be noted that higher temperatures may increase the operating cost of the furnace and promote unacceptable grain growth in the carburised part. Although gas consumption in the furnace is expected to increase with an increase in furnace temperature, this effect may be offset by shortening the total carburising time. A compromise must therefore be reached between the required carburising rate and case depth, the microstructure (and properties) of the carburised part and the maintenance costs of the furnace.

2.6 GRAIN SIZE

As stated earlier, an increase in carburising temperature may promote grain growth if not offset by a reduction in carburising time. Considerable grain growth has been observed in carburised steels treated at elevated temperatures [31,32]. Grain growth during carburising may influence a number of bulk material properties, such as strength, impact toughness, creep strength and fatigue resistance. As shown in equation (2.19), the Hall-Petch equation relates yield strength, σ_y, to the average grain diameter, d. This relationship indicates that the yield strength increases with a reduction in grain size [33].

$$\sigma_y = \sigma_0 + k.d^{-½} \quad \ldots(2.19)$$

where σ_0 and k are constants.

Grain boundaries act as obstacles to the movement of dislocations. A dislocation that attempts to pass from one grain to another has to change its direction of movement due to

crystallographic misorientation between adjacent grains. This tends to promote the pile-up of dislocations at grain boundaries. A fine grained material has more grain boundary area and generally displays higher yield strength than coarse grained material as higher applied stress is needed to cause slip through the boundary [34].

The driving force for grain growth is a reduction in the surface energy of the grain boundaries. Grain growth is promoted by higher temperatures as more thermal activation energy is available for the migration of the grain boundaries. As grain growth occurs at elevated temperatures, the overall number of grains is reduced as larger grains consume smaller grains. The Ideal Grain Growth Law relates the average grain diameter, D, to the initial grain size, D_0, as shown in equation (2.20) [34,35].

$$D^2 - D_0^2 = kt \qquad \ldots(2.20)$$

where k is a proportionality constant and t is the holding time at temperature.

An Arrhenius-type equation describing the proportionality constant K is shown in equation (2.21). This confirms that grain growth accelerates at higher temperatures due to an increase in the value of k. Excessive grain growth can be offset to a certain extent by reducing the total carburising time, t, required to achieve a specified case depth [34].

$$k = k_o \exp(-Q/RT) \qquad \ldots(2.21)$$

where k_o is a constant, T is temperature (K), Q is the activation energy for grain growth, and R is the universal gas constant.

The Ideal Grain Growth Law is often written in a more general form by substituting the variable m as the exponent in the equation (shown in equation (2.22)).

$$D^m - D_0^m = kt \qquad \ldots(2.22)$$

It has been shown experimentally that the value of m lies within a range of two to five. In an ideal system controlled by diffusion, the kinetic exponent, m, has a value of two (as shown in equation (2.20)) [36]. An exponent of three implies that the presence of precipitates or inclusions plays a role in controlling the grain size by pinning grain boundaries. Exponent values higher than three suggest that precipitates and grain boundary diffusion play a role in determining the grain size [37].

The preceding discussion suggests that the total carburising time may be reduced by increasing the carburising temperature. Such an increase in temperature may, however, affect the case depth and surface hardness, give rise to uncontrolled grain growth in the carburised part and affect the dimensions and level of distortion during subsequent heat treatment. This project investigated the feasibility of increasing the carburising temperature with the aim of reducing the total carburising time, increasing production rates and reducing gas consumption in the furnace. Chapter 3 examines the objectives of this investigation in more detail.

CHAPTER 3 - OBJECTIVES

Gears are critical components that play a significant role in determining performance and reliability in the aerospace industry. Various heat treatment steps are required during the production of precision gears to achieve the specified surface hardness, core toughness and part dimensions. A typical heat treatment cycle for precision gears is comprised of three stages: carburisation to increase the surface carbon content, hardening and quenching to form martensite, and tempering to improve ductility and toughness [38].

This investigation focused on the carburisation heat treatment, and utilised an industrial vacuum carburising furnace and acetylene atmosphere to study the effect of carburising temperature on the properties of the carburised surface layer. The project aimed to determine whether the total carburising time could be decreased by increasing the carburising temperature, without adversely affecting the specified case depth and hardness values. The predictions of published carbon diffusion models (taking into account the influence of temperature, changing carbon concentration and alloying element content on the diffusion coefficient of carbon in austenite) were compared with the carbon concentration profiles measured after carburising at different temperatures.

An increase in carburising temperature is likely to increase the diffusion rate of carbon and reduce the total carburising time required to achieve a specified case depth and surface hardness. Such a reduction in carburising time should reduce gear production times and may decrease gas consumption during heat treatment. Higher temperatures may, however, result in unacceptable grain growth during heat treatment or excessive dimensional changes after quenching due to the high quenching stresses generated in the part.

In order to examine the feasibility of reducing the total carburising time by increasing the carburising temperature, this project had the following objectives:

- To determine the influence of carburising temperature on the case depth and surface hardness of carburised samples.
- To determine whether published diffusion models for carbon in austenite are suitable for predicting carbon concentration profiles during gas carburising.
- To compare the measured carbon concentration profiles with carbon contents predicted on the basis of temperature, changing carbon concentration and steel alloying element content.
- To study the influence of carburising temperature on the grain size; microstructure, specimen dimensions and mechanical properties of the vacuum remelted low carbon carburising steel used in the commercial production of precision gears.

The experimental procedure used during the course of this investigation to achieve these objectives is described in more detail in Chapter 4.

CHAPTER 4 - EXPERIMENTAL PROCEDURE

This chapter describes the experimental procedure followed during the course of this investigation, with specific focus on the preparation of the carburising test pieces, the vacuum carburising furnace used, the testing and calibration procedures followed and the carburising and heat treatment parameters applied.

4.1 TEST PIECE PROPERTIES

In order to evaluate the influence of test parameters on carburising efficiency, standard test bars, machined from a single batch of Latrobe Lescalloy® 16NCD13 VAC-ARC carburising steel, were used. This steel is used commercially in the production of precision gears. 16NCD13 VAC-ARC is a vacuum remelted low alloy carburising steel. In the carburised condition, it features high case hardness in combination with high impact and fracture toughness in the core structure. Its superior cleanliness makes 16NCD13 suitable for use in critical aerospace and actuator applications [39]. The typical chemical composition of the steel is shown in Table 4.1 and the specified mechanical properties in Table 4.2.

Table. 4.1. *Typical chemical composition range specified for 16NCD13 VAC-ARC® low alloy carburising steel (weight percentage; balance Fe) [39].*

Element	*%C*	*%Mn*	*%Si*	*%S*	*%P*	*%Cr*	*%Ni*	*%Mo*	*%Cu*
Minimum	0.12	0.30	0.15	-	-	0.80	3.00	0.20	-
Maximum	0.17	0.60	0.40	0.010	0.015	1.10	3.50	0.30	0.35

Table 4.2. *Specified mechanical properties of 16NCD13 after hardening and tempering [39].*

Tensile Strength (MPa)	*Yield Strength (MPa)*	*%Elongation*
1180 - 1380	≥ 980	≥ 8

A representative test sample was analysed using spark emission spectroscopy and the chemical composition shown in Table 4.3 obtained. This confirms that the composition of the test samples used in this investigation is within specification for the 16NCD13 carburising material used in the preparation of commercial parts.

Table. 4.3. *Chemical composition of the 16NCD13 VAC-ARC test samples used in this investigation (weight percentage; balance Fe).*

%C	*%Mn*	*%Si*	*%S*	*%P*	*%Cr*	*%Ni*	*%Mo*	*%Cu*
0.15*	0.478	0.229	0.010	0.015	1.033	3.478	0.25	0.132

* Inert gas fusion (Leco™) analysis yielded a carbon content of 0.165%.

Two test bar geometries were used for the collection of carburising data. The first type of sample was a standard V-type test piece, shown in Figure 4.1. The V-type test piece is used to simulate a gear profile, i.e. the tip (peak), flank and root of the gear tooth. The standard round bar specimen, shown in Figure 4.2, was used to determine the carbon profile of the carburised part. In each trial three carburising test pieces and one test piece subsequently

used to determine the change in carbon composition with distance below the carburised surface (Figure 4.2) were included in the furnace load which was made up of scrap material to simulate a standard load of about 30 to 50 kg. The low carburising volumes are typical of the application, which is geared towards specialised parts.

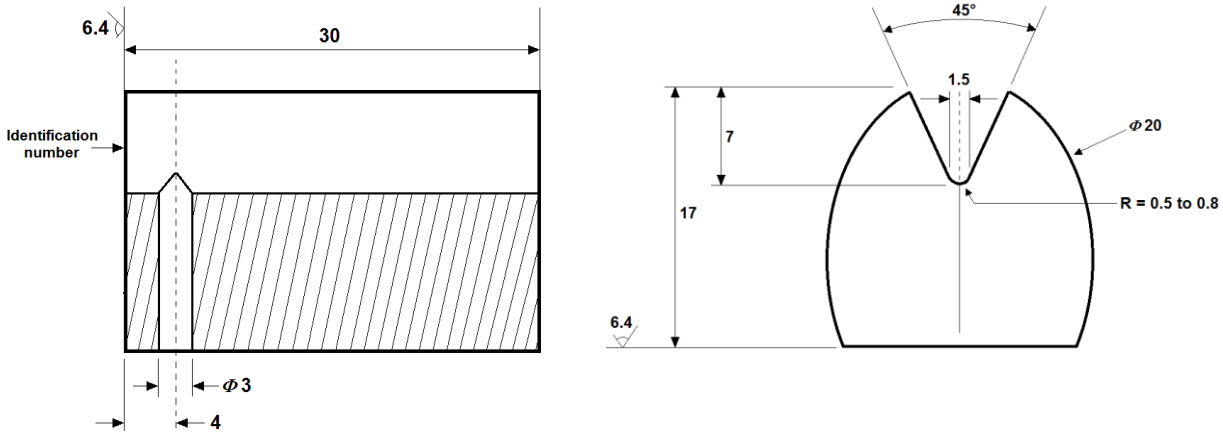

Figure 4.1. *Standard V-type test piece used in this investigation to simulate the carburising of gears (all dimensions in mm).*

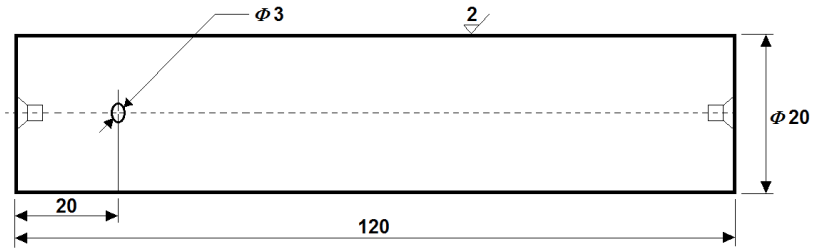

Figure 4.2. *Standard round bar test piece used in this investigation to determine the carbon profile after carburising (all dimensions in mm).*

Cylindrical tensile samples were machined from the 20 mm diameter round test pieces in accordance with the specifications in ASTM A370-14 [40]. The dimensions of the tensile samples are given in Figure 4.3 and Table 4.4.

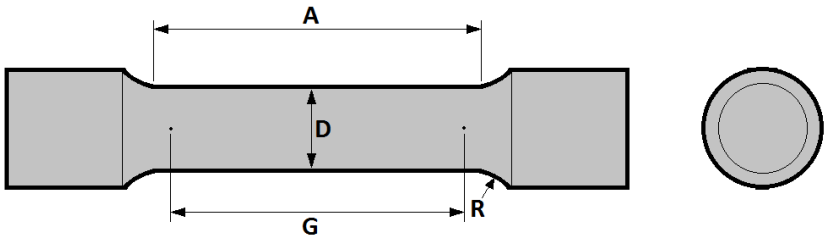

Figure 4.3. *Dimensions of cylindrical tensile samples.*

Table 4.4. *Actual dimensions of cylindrical tensile samples used in this investigation.*

Nominal diameter	*Gauge length (G)*	*Diameter (D)*	*Radius of fillet (R)*	*Length of reduced section (A)*
4.0 mm	16.0 ± 0.10 mm	4.0 ± 0.08 mm	minimum 4.0 mm	minimum 20.0 mm

4.2 THE VACUUM CARBURISING FURNACE

The Ipsen Avac 524™ furnace used during this investigation is a single chamber vacuum furnace with an internal furnace working space of 600 mm x 900 mm x 600 mm (see Figure 4.4). The furnace is capable of either convection heating (in the range of 150°C to 850°C) or heating under vacuum (in the range of 500°C to 1320°C). The internal furnace pressure can be varied from 1000 mbar to 10^{-5} mbar, while the low pressure range (during low pressure carburising) can be controlled between 10^{-2} mbar and 1 mbar. The pressure during convection heating can be varied between 1200 and 2000 mbar, and the maximum gas quench pressure is 10 bar (nitrogen).

Figure 4.4. *The Ipsen Avac 524™ vacuum furnace used during the course of this investigation.*

The carburising process was controlled by the Ipsen Vacu-Prof™ control system and twelve type R (Pt/Pt-10%Rh) thermocouples were used to monitor the temperature within the furnace during testing.

4.3 REPEATABILITY

In the automotive and aerospace industries the repeatability of any manufacturing process is important to ensure that the required product quality is maintained. Furnace calibration and regular testing were therefore carried out to ensure repeatability of the experiments. The following calibration tests were performed, based on the requirements described in AMS 2750E [41]:

- Leak test (weekly).
- Temperature Uniformity Survey (TUS) (every 3 months).
- System Accuracy Testing (SATS) (every 3 months).
- Uniformity Testing (every 6 months).

These tests are briefly described below.

4.3.1 *Leak Test:*

During leak testing a full carburising cycle is run and the furnace allowed to cool to below 80°C. This ensures that the chamber reaches a vacuum pressure below 50 μm Hg or 6.66×10^{-2} mbar. Once the furnace temperature falls below 80°C, the carburising cycle is interrupted which closes all the furnace valves and stops the vacuum pumps. The pressure in the furnace is then recorded as a function of time. Readings are manually recorded at 5, 10, 15 and 30 minute intervals. The leak rate of the furnace can be calculated by means of equation (4.1) and should not exceed 20 μm Hg per hour (or 2.66×10^{-2} mbar per hour).

Leak rate = (Last reading – First reading)/Elapsed time in hours …(4.1)

4.3.2 *Temperature Uniformity Test (TUS):*

Temperature Uniformity Tests are a series of tests during which calibrated field test instrumentation and sensors are used to measure temperature variations within the qualified furnace work zone prior to and after thermal stabilisation. Testing is carried out in accordance with AMS 2750E [41]. In the case of the Ipsen Avac 524 vacuum furnace (a class 5 furnace), the temperature range specified for testing is 540°C to 980°C with a permissible variation of ±14°C. The standard requires the use of a minimum of eight thermocouples as the furnace working area is larger than 0.085 m^3. Twelve thermocouples were used during this investigation.

4.3.3 *System Accuracy Test (SAT):*

The System Accuracy Test involves comparison of the sensor and instrument readings with values or readings taken using calibrated test instruments to determine if the measured deviations are within applicable limits. The test is performed to ensure the accuracy of the furnace control and recorder systems in the working zone. Testing is carried out in accordance with the requirements of AMS 2750E [41].

4.3.4 *Uniformity Testing:*

Uniformity testing was carried out to detect any variations in carburising efficiency in the furnace working space. Nine test pieces were loaded onto a large test frame as shown in Figure 4.5. Thermocouples were attached to the test samples.

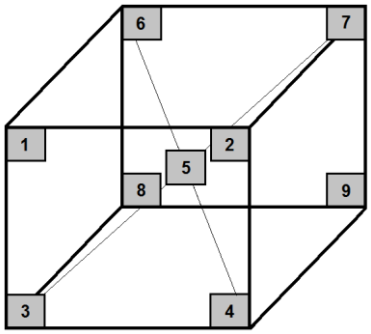

Figure 4.5. *Schematic illustration of the location of test samples during uniformity testing in the furnace.*

The furnace was programmed to deliver a case depth of 0.55 mm to 0.65 mm, and surface hardness and core hardness values ranging from 675 to 773 HV_5 and 366 to 440 HV_{30}, respectively. The samples were carburised at 900°C for a total carburising time of 2 hours and 30 minutes. The test pieces were cooled to 850°C followed by gas quenching at a rate of 80°C per minute to a temperature of 60°C. After carburising the samples were austenitised (at 820°C), quenched and tempered at 140°C. (Refer 4.4)

Nine carburising and nine carbon potential test pieces are usually examined during uniformity testing. On completion of the carburising and final heat treatment cycles the samples are tested for the following:

- Carbon concentration at depths of 0.1 mm, 0.2 mm and 0.3 mm below the surface.
- Case depth obtained at the outer diameter, flank and root of simulated gear profiles.
- Case depth variation (should be less than 0.05 mm between the nine samples).
- Surface and core hardness.

The results of the uniformity test performed during this project are shown in Table 4.5.

Table 4.5. *Uniformity test piece results.*

Sample	*Surface hardness (HV_5)*	*Core hardness (HV_{30})*	*Case depth (mm)**			*Subsurface hardness (HV)*			*% Carbon Results*		
			Outer Ø	*Flank*	*Root*	*Outer Ø*	*Flank*	*Root*	*0.1 mm*	*0.2 mm*	*0.3 mm*
1	721; 710	425; 428	0.58	0.57	0.57	717	713	723	0.70	0.67	0.63
2	739; 729	430; 432	0.57	0.59	0.57	702	705	703	0.71	0.67	0.62
3	727; 728	424; 430	0.59	0.59	0.59	725	705	732	0.72	0.68	0.63
4	729; 730	431; 433	0.59	0.59	0.60	705	700	705	0.69	0.67	0.61
5	713; 721	431; 433	0.58	0.61	0.58	721	725	731	0.69	0.68	0.57
6	726; 725	430; 430	0.62	0.60	0.60	694	713	700	0.69	0.68	0.62
7	731; 724	426; 428	0.58	0.59	0.56	713	701	721	0.69	0.65	0.61
8	733; 717	429; 432	0.58	0.59	0.60	707	707	713	0.70	0.68	0.63
9	734; 738	427; 432	0.58	0.59	0.58	724	715	711	0.69	0.67	0.63
Required	**625 - 773**	**366 - 440**	**0.55 - 0.65**			**For information only**			**0.65 - 0.9**	**0.60 - 0.9**	**0.50 - 0.9**

* A variation 0.05 mm or less was obtained by subtracting the highest and lowest values (Required ≤ 0.05 mm).

4.4 PROCESS PARAMETERS

In order to evaluate the influence of carburising temperature on carburising efficiency, the following process parameters were used in the collection of test data:

- Carburising atmosphere: Acetylene (C_2H_2)
- Carburising temperature: 900°C to 960°C
- Annealing cycle: 670°C for 3 hours
- Austenising temperature: 820°C for 45 minutes
- Quenching method: High pressure gas quench (HPGQ) at 10 bar N_2
- Tempering 140°C for 3 hours

The carbon potential of the furnace atmosphere was maintained at a maximum of 1.43% to ensure a maximum surface carbon concentration of between 0.8% and 0.9%. An annealing cycle was included to simulate the current commercial gear machining process as closely as possible. The annealing cycle is carried out to ensure ease of machining or grinding of carburised gears prior to the hardening and tempering cycle.

The carburising temperature was increased in intervals of 20°C for each trial, from a minimum of 900°C to a maximum of 960°C. As shown in Table 4.6, the carburising time was adjusted for each temperature to maintain a constant case depth of 0.5 mm. All other process parameters were kept constant to evaluate the effect of increased temperature on the case hardness and microstructure.

Table 4.6. *Reduction in the duration of the carburising cycle with an increase in carburising temperature.*

Temperature (°C)	*Carburising time at temperature (minutes)*
900	104
920	95
940	64
960	44

The carbon profile in the test piece or part after carburising plays an important role in determining the properties of the part. The highest carbon concentration should be at the surface of the component, with the carbon content gradually decreasing towards the core of the test piece or part. The surface concentration is usually equal to the eutectoid carbon content (or slightly higher). The eutectoid carbon concentration is, however, reduced by the addition of alloying elements to the steel. Figure 4.6 shows the effect of additions of titanium, molybdenum, tungsten, silicon, chromium, manganese and nickel on the eutectoid composition in steel [42].

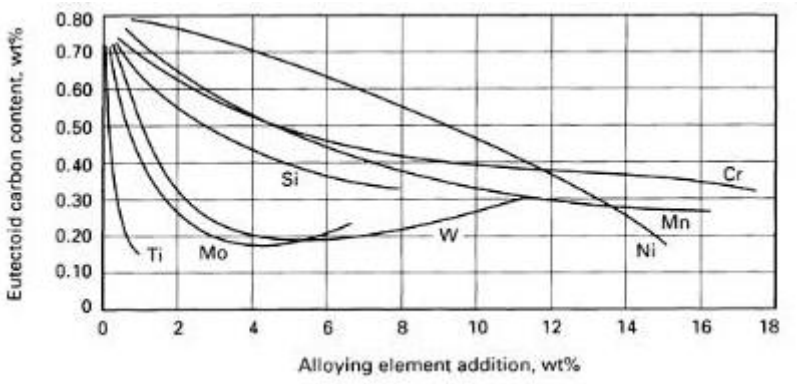

Figure 4.6. *The influence of alloying additions on the eutectoid composition in steel [42].*

The effect of the alloying elements on the diffusivity of carbon in austenite was quantified using the parameter *q*, calculated as a function of alloy content by means of equation (2.13).

4.5 THE CARBURISING PROCESS

The low pressure gas carburising (LPGC) treatment of precision gears involves a number of steps. At the start of the process, the machined parts that require processing are loaded into the furnace and the furnace chamber is evacuated. The pressure is reduced to below $7x10^{-1}$ mbar and once excess oxygen has been removed, the control programme initiates the increase in furnace temperature. The temperature is raised to 650°C, then to 850°C at a nitrogen pressure of 2 bar with the parts heated by convection. The test pieces are soaked just long enough at temperature to ensure uniform heating. On completion of the soak time at 850°C the vacuum furnace removes the nitrogen (pressure in the furnace is reduced to below 1 mbar) from the holding chamber and the temperature begins to rise to the set carburising temperature.

Once the required carburising temperature is reached, acetylene is added to the furnace atmosphere and the carburising process is initiated. The pressure in the vacuum furnace at temperature is usually in the region of $1x10^{-1}$ mbar. During the "boost" stage carbon is absorbed by the austenite and hydrogen is liberated. Due to carbon saturation in the austenite the addition of acetylene is interrupted after a specified time to allow the diffusion of the carbon into the part. Acetylene is evacuated from the furnace during the diffusion cycle.

During the first diffusion stage carbon migrates into the steel towards the core of the test piece, and the surface carbon content decreases. The next stage of carburising then starts with successive "boosts" of carbon, followed by diffusion, until the required case depth is obtained. Typical carburising temperature and pressure cycles are shown in Figure 4.7.

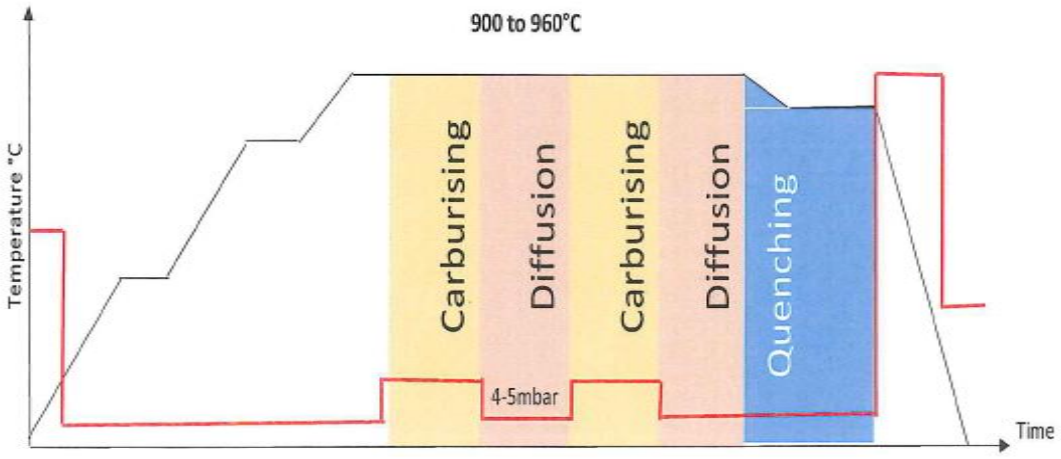

Figure 4.7. *Typical temperature and pressure cycles during carburising [43].*

Once the full carburising cycle is completed the temperature is reduced to 850°C and the furnace charge is rapidly cooled in an argon atmosphere at a programmed rate of 60°C to 65°C per minute. After cooling the parts are removed from the furnace and placed into a second vacuum furnace where the components are annealed prior to grinding of the gear profiles to the required dimensional tolerances. The process involves heating of the parts to a temperature of 670°C, holding at temperature for approximately three hours, followed by gas or fan cooling in a nitrogen atmosphere at 1.2 bar.

Once final machining has been completed, the parts are austenitised at 820°C and quenched in nitrogen at 10 bar pressure. Tempering is then performed at 140°C for 3 hours to reduce residual stresses and to introduce some ductility and toughness.

4.6 DERIVING THE GAS FLOW RATE TO VERIFY GAS CONSUMPTION

Increasing the carburising temperature is expected to increase gas consumption due to the higher carbon diffusion rates. This effect may be offset to some extent by the decrease in carburising time shown in Table 4.6. A method for deriving the actual flow rate of the carburising gas to provide the required amount of carbon for a given furnace load was proposed by Antes [44]. The proposed method calculates the required theoretical gas flow rate on the assumption that all acetylene dissociates in the furnace. The theoretical flow rate of the gas during the boost cycle therefore does not consider the actual fraction acetylene that dissociates.

To calculate the carburising gas flow rate, the following parameters are required:

- the total surface area to be carburised,
- the desired depth of the carburised layer, and
- the volume of the material to be carburised (based on area and carburising depth).

Antes further proposed that in determining the amount of carbon required to carburise a calculated volume, the following values are required:

- the molecular weight of the gas, and
- the chemical dissociation reactions that would provide the amount of carbon required if the total boost or carburising time is available.

Based on the dissociation reaction of acetylene, described in §1.3, the final theoretical gas flow rate ($F_{theoretical}$) can be calculated using equation (4.2).

$$F_{theoretical} = (\text{total carbon required} \times 0.0787) / (\text{total boost} \times 0.0011) \quad \ldots(4.2)$$

Equation (4.2) assumes that acetylene dissociates completely. The real flow rate can be calculated as the final theoretical gas flow rate divided by the fraction acetylene that actually dissociates.

4.7 EVALUATION OF QUENCH MEDIA

During the course of this investigation, trials were also performed to evaluate the efficiency of the gas quenching process performed after austenitising as part of the gas carburising process. Initial trials were performed at 900°C. Further trials were conducted at 920°C during which two sets of test pieces were carburised and hardness profiles measured at the outer diameter, flank and root of the samples. Both sets of test pieces were carburised, hardened and quenched using either the hardening cycle in the vacuum furnace, followed by high pressure gas quenching, or austenitising in a salt bath followed by agitated oil quenching. The quenching process promotes transformation to martensite.

The quenching efficiency of the two quenching media varies due to differences in their physical properties. During quenching in a liquid the cooling process takes place in three stages, described below and shown schematically in Figure 4.8. Each stage is associated with a change in heat transfer coefficient [1,45].

- Vapour-blanket cooling stage: During this stage, vaporisation of the liquid occurs due to the high surface temperature of the component being quenched. A thin vapour film is formed in contact with the part surface and cooling occurs by means of conduction and radiation.
- Vapour-transport cooling stage: As the temperature of the part decreases to about 700°C, the vapour blanket (film) becomes unstable. The quench medium comes into direct contact with the metal surface and boiling occurs. Rapid convective heat transfer takes place.
- Liquid cooling stage: Active boiling ceases and further cooling of the metal surface occurs by convection.

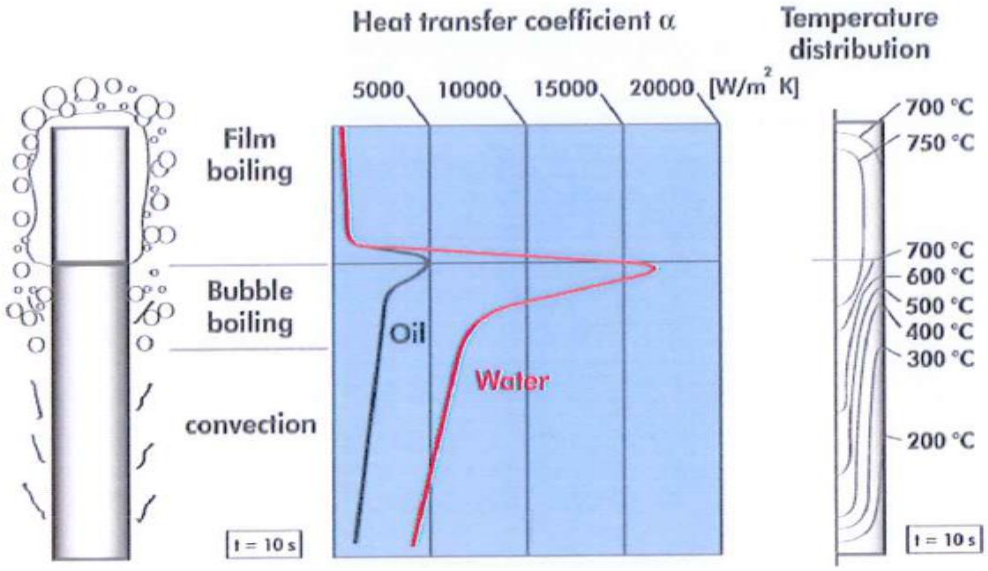

Figure 4.8. *Schematic illustration of the liquid phase quenching process [46].*

During gas quenching, shown schematically in Figure 4.9, no phase changes occur in the quenching medium and cooling is mainly by convection. The heat transfer coefficient remains relatively unchanged. More uniform heat extraction is obtained, reducing the amount of distortion on cooling [47].

The gas quench rate is determined by the heat transfer coefficient (α) and is dependent on both the pressure ($\rho_{0.7}$) and flow velocity ($\omega_{0.7}$) of the gas. This relationship is shown in equation (4.3), where C is a constant [48].

$$\alpha = C\omega_{0.7}.\rho_{0.7} \quad (W.m^{-2}.K^{-1}) \qquad \ldots(4.3)$$

In a recent study [45] equation (4.3) was modified to take into account the component diameter (d), the viscosity of the gas (η), as well as the specific heat capacity (C_p) and the thermal conductivity (λ) of the gas. The modified relationship is shown in equation (4.4).

$$\alpha = C\omega_{0.7}\rho_{0.7}d^{-0.3}\eta^{-0.39}C_p^{0.31}\lambda^{0.69} \quad (W.m^{-2}.K^{-1}) \qquad \ldots(4.4)$$

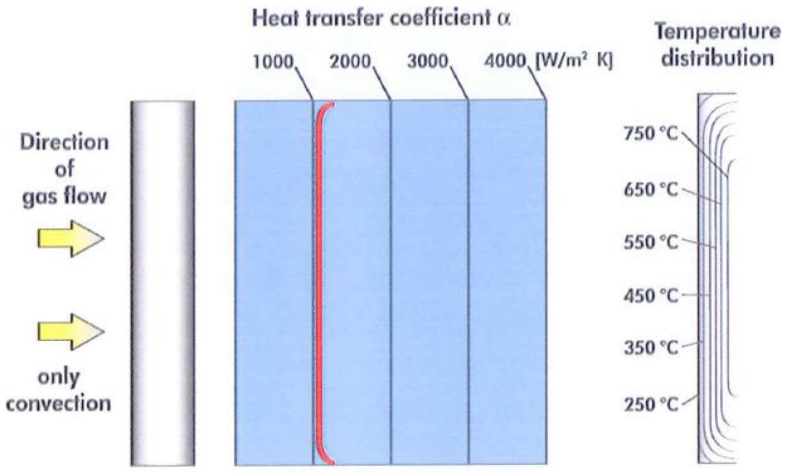

Figure 4.9. *Schematic illustration of the gas quenching process [46].*

The relative quenching capacity (cooling rate) of various gas quenching media is shown in Figure 4.10. Gas quenching in nitrogen after austenitising was used during this investigation.

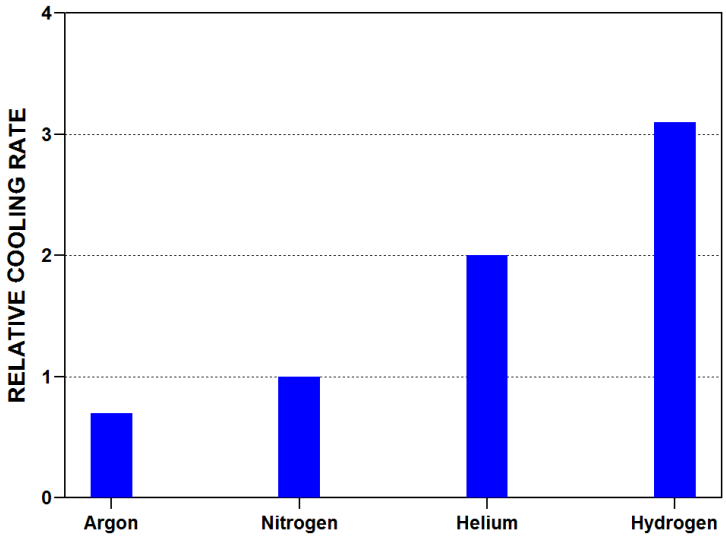

Figure 4.10. *Relative cooling rate in various gas quenching media [49].*

4.8 PHYSICAL PROPERTIES

Graphs predicting the carbon concentration profiles and case depths for the test samples were obtained using Avac™ simulation software and compared with the actual test results obtained. The Avac™ simulation program is used to keep pretesting to a minimum [50] by creating low pressure carburising programs which calculate carbon transfer and diffusion based on acetylene characteristics. Key process parameters, including temperature, surface carbon content and case depth are entered into the simulation program and automatically transferred to the furnace controller. The carbon profiles are then calculated by the simulation program using the temperature, surface carbon content and case depth requirements.

While the aim of this project was to ensure that the correct case depth and surface hardness values were maintained at increased carburising temperatures, the effect of carburising temperature on bulk tensile properties was also considered due to the risk of grain growth at higher temperatures. The dimensions of the tensile samples were shown in Figure 4.3 and Table 4.4. The test pieces were prepared using the process described in §4.4, i.e. carburising, annealing, machining (into test pieces) and final hardening and tempering.

The test results were used to confirm the effectiveness of the Avac™ simulation program, to confirm the feasibility of using increased carburising temperatures to reduce production times and to determine the applicability of Fick's Law and the proposed diffusivity models. These results are considered in more detail in Chapter 5.

CHAPTER 5 - RESULTS AND DISCUSSION

5.1 MEASURED CARBON PROFILES COMPARED WITH SIMULATED MODELS

As with most modern equipment, variations in results are sometimes a direct result of poor calibration or problems associated with human error. While determining the actual carbon profiles of the carburised test pieces, it was also of interest to determine the variation between the actual measured results and those predicted by the furnace control programme. This was done by carburising a cylindrical test piece (using the procedure described in Chapter 4) to the required case depth. After carburising the test piece was annealed (to facilitate machining) and the carbon content was measured at various depths below the surface. The carbon profiles were obtained by removing sample material in steps of 0.1 mm to 1.0 mm below the surface, as well as at depths of 2.0 and 3.0 mm below the surface, and analysing the carbon content of the shavings. The resultant carbon concentration values were compared to the predicted values.

This enabled accurate appraisal of the following parameters:

- the carbon content at the surface,
- the carbon profile,
- the carbon content as a function of case depth,
- the carbon content at the core, and
- the variation between predicted and actual carbon contents as a function of depth below the surface.

The comparison between predicted carbon concentration profiles and actual measured results is shown in Figures 5.1(a) to (d) for carburising temperatures of 900°C to 960°C. The average variation between the measured and predicted carbon concentrations at each carburising temperature is shown in Table 5.1. It is evident that the Avac™ simulation programme predicts the carbon concentration profiles well. The variation between the simulated and measured results increases with an increase in carburising temperature.

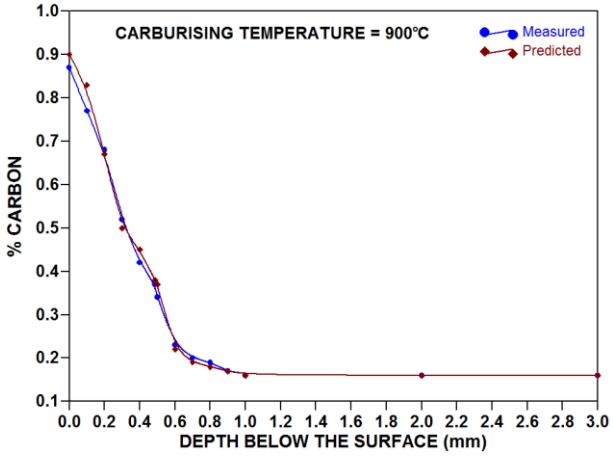

(a)

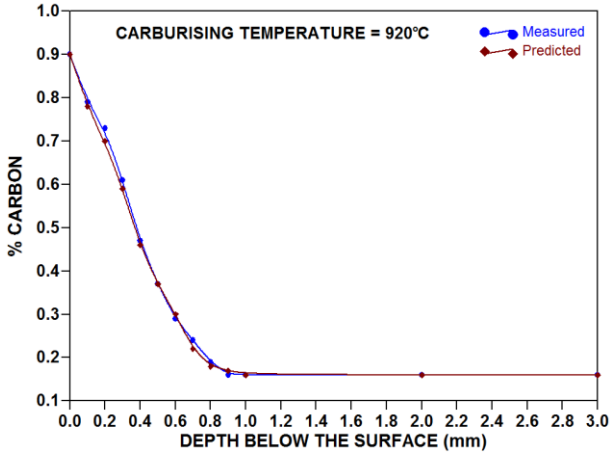

(b)

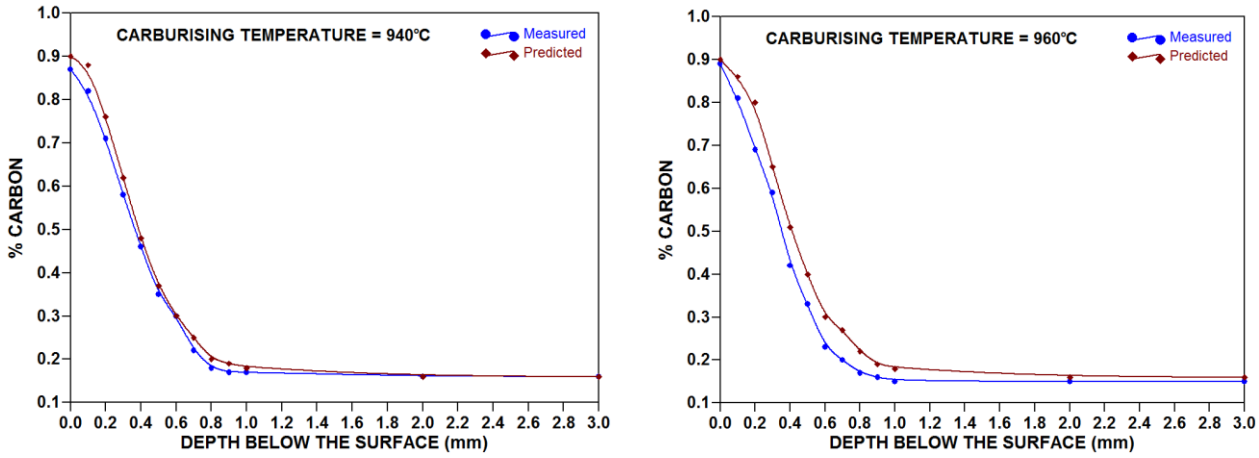

Figure 5.1. *Simulated carbon profiles compared with experimental carbon concentration values for carburising temperatures (and times) of: (a) 900°C (104 min.); (b) 920°C (95 min.); (c) 940°C (64 min.); and (d) 960°C (44 min.).*

Table 5.1. *Average variation between the simulated and experimentally measured carbon concentration values as a function of carburising temperature.*

Temperature	*900°C*	*920°C*	*940°C*	*960°C*
% Variation	2.9	2.6	5.4	14.0

Figure 5.2 compares the measured carbon concentration profiles for each of the carburising temperatures evaluated. The shape of the curves obtained is typical of carbon concentration profiles in carburised materials. Figure 5.2 therefore confirms that increasing the carburising temperature, while at the same time reducing the carburising time (Table 4.6), results in similar concentration profiles and case depths.

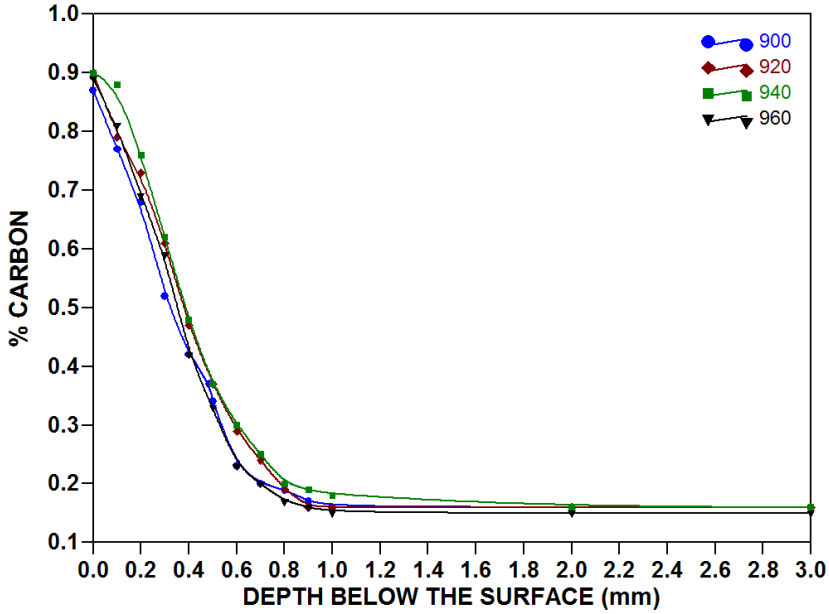

Figure 5.2. *Carbon concentration profiles measured for different carburising temperatures and carburising times.of: (a) 900°C (104 min.); (b) 920°C (95 min.); (c) 940°C (64 min.); and (d) 960°C (44 min.).*

5.2 THE EFFECT OF INCREASED TEMPERATURE ON CARBURISING TIME

It is generally recognised that increasing the carburising temperature reduces the time required to process the part. This can be attributed to an increase in carbon diffusion rate with an increase in temperature. Each carburising temperature tested during the course of this investigation was reviewed and based on the actual case depth achieved and the carburising time required, the carbon diffusion rate was calculated as a function of carburising temperature (as shown in Figure 5.3).

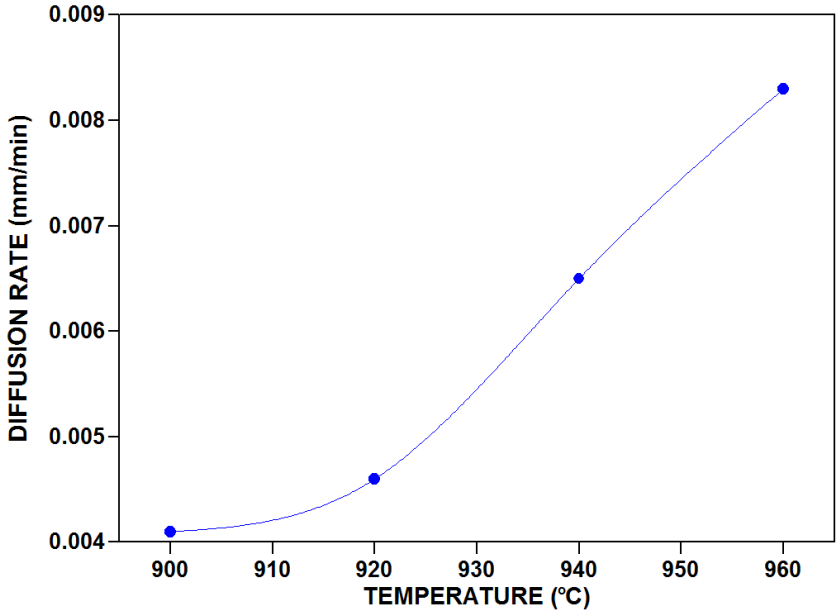

Figure 5.3. *Calculated diffusion rate as a function of carburising temperature.*

A comparison between the standard commercial carburising cycle (performed at 900°C) and carburising at higher temperatures indicates that at 960°C, the total carburising cycle could be shortened by almost 53%, as shown in Table 5.2. This can be attributed to the increased diffusion rate of carbon at higher temperatures. A decrease in processing time can potentially benefit industry by reducing carburising times and decreasing the cost associated with the treatment process. It is, however, important that the increase in carburising temperature does not have a detrimental effect on the properties of the carburised case and the core material.

Table 5.2. *Reduction in the total duration of the carburising cycle with an increase in carburising temperature.*

Temperature (°C)	*Carburising time at temperature (minutes)*	*Diffusion time (minutes)*	*Total time (minutes)*	*Total cycle time (minutes)*	*Calculated Diffusion Rate (case depth and time) ($m^2.s^{-1}$)*
900	104	15	104	246	$3,99X10^{-7}$
920	95	13	95	220	$5,27X10^{-7}$
940	64	14	64	209	$6,16X10^{-7}$
960	44	13	44	188	$8,75X10^{-7}$

5.3 EFFECT OF INCREASED TEMPERATURE ON HARDNESS

In order to determine the hardness of carburised samples, a calibrated Vickers micro-hardness tester was used to measure hardness profiles from the surface of carburised test pieces to a depth of 1 mm below the surface. A typical hardness traverse is shown in Figure 5.4.

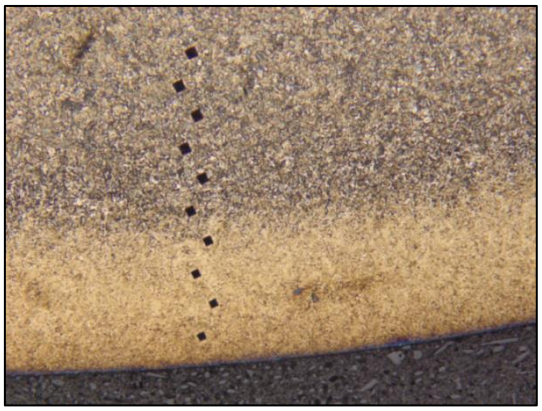

Figure 5.4. *A typical hardness traverse from the surface of a carburised specimen (50x magnification).*

The average hardness values at various depths were used to construct hardness profiles as a function of depth below the surface, shown in Figure 5.5. Except for a marginally lower surface hardness after carburising at 900°C, no significant differences between the hardness profiles constructed at different carburising temperatures were observed.

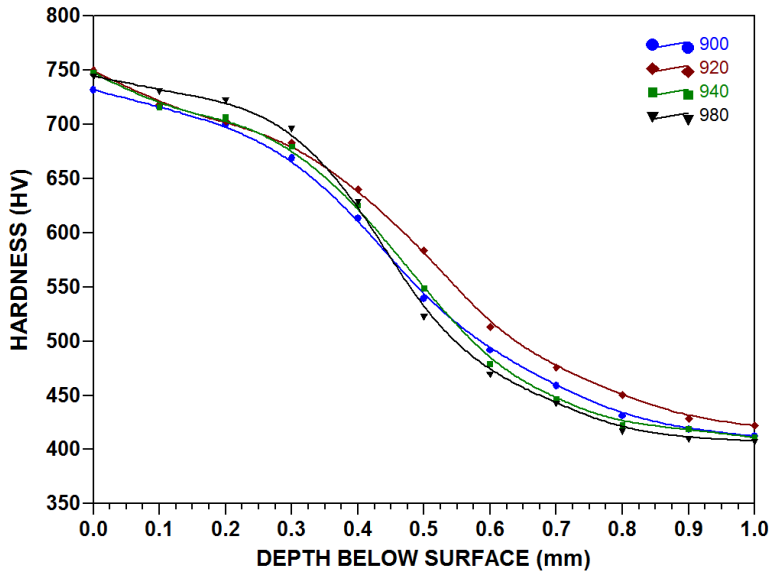

Figure 5.5. *Hardness as a function of depth below the surface for different carburising temperatures.*

For samples treated using high pressure gas quenching, further hardness measurements were taken across polished test samples to determine the uniformity of the carburising process, particularly at the flank and root of simulated gear profiles. The correlation between hardness and case depth for carburised test pieces, at the flank and root positions, are shown in Figures 5.6(a) and (b) for carburising temperatures of 920°C and

940°C, respectively. It is evident that the hardness profiles measured at the flank and root positions after carburising at 920°C and 940°C are very uniform. As a point of reference, a root-to-flank case depth ratio of approximately 65% [51] is typical after gas carburising. Figure 5.6 shows a ratio of greater than 90%, confirming the effectiveness of the process.

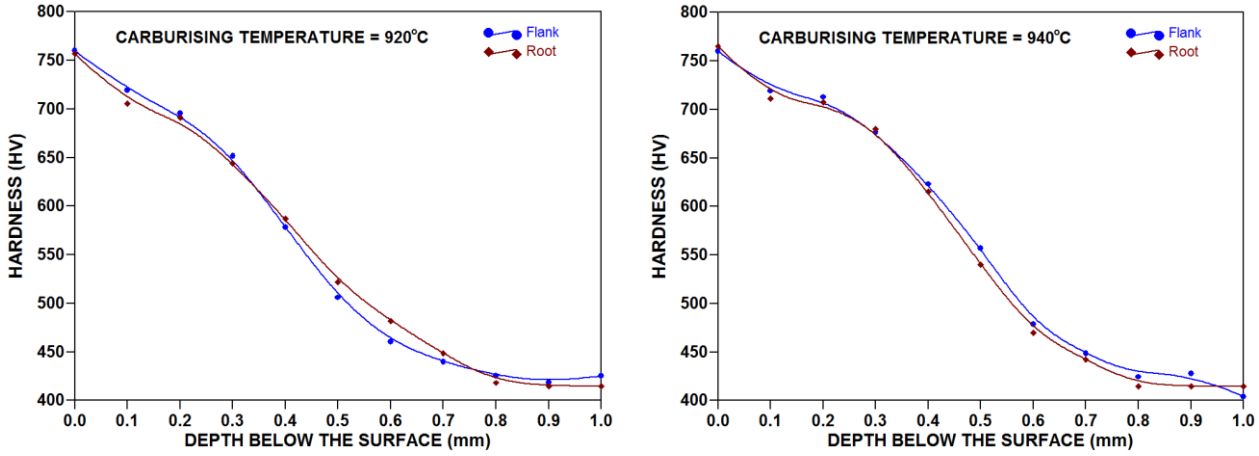

(a) (b)

Figure 5.6. *Hardness comparison at the test piece root and flank after carburising at 920°C and 940°C.*

5.4 INFLUENCE OF QUENCHING MEDIUM ON HARDNESS AND CASE DEPTH

To evaluate the effectiveness of the high pressure gas quench used during the commercial carburisation process, test pieces were subjected to gas carburising at 900°C, followed by annealing at 670°C for 3 hours and gas/fan cooling to room temperature. The test samples were then either austenitised in a vacuum furnace at 820°C for 45 minutes, followed by high pressure gas quenching (10 bar nitrogen), or austenitised in a salt bath at 820°C for 15 minutes and oil quenched. The oil temperature was maintained at 30 ± 3°C.

Both sets of samples were then tempered in a vacuum furnace at 140°C for two hours and allowed to cool in air to room temperature. The surface and core hardness values and the case depth were measured for each sample, as shown in Table 5.3. Actual parts (gears) were also subjected to the same process, with the results shown Table 5.4.

Based on the data obtained the root-to-flank hardness ratio, as well as a correlation factor between the predicted and measured results, were determined (shown in Table 5.5). The test results confirm the findings reported in §5.3, and show that the root-to-flank hardness ratios obtained are still well above that required for gas carburising. Measurement of the root, flank and surface hardness values were performed on test pieces carburised at 920°C and hardened either in a salt bath followed by oil quenching, or in a vacuum furnace followed by high pressure gas quenching. The results are shown in Table 5.6 and illustrated graphically in Figure 5.7.

Table 5.3. *Average hardness and case depth measurements obtained in test samples for different quenching media at 900°C.*

Test Requirements	*Test piece preparation*		*Specification requirements*
	High pressure gas quench	*Oil quench*	
Surface hardness (HV_5)	731 HV	734 HV	655 - 770 HV
Core hardness (HV_{30})	414 HV	426 HV	321 - 430 HV
Effective case depth at 550 $HV_{0.5}$			
Outer *Ø*	0.50 mm	0.50 mm	0.45 - 0.55 mm
Flank	0.48 mm	0.50 mm	
Root	0.47 mm	0.47 mm	
Hardness at 0.1 mm depth ($HV_{0.5}$)			
Outer *Ø*	716 HV	699 HV	Information only
Flank	733 HV	702 HV	
Root	709 HV	693 HV	
Microstructure	Satisfactory	Satisfactory	Martensitic

Table 5.4. *Average hardness and case depth measurements obtained in gears for different quenching media at 920°C.*

Test Requirements	*Gear preparation*		*Specification requirements*
	High pressure gas quench	*Oil quench*	
Surface hardness (HV_5)	738 HV	745 HV	655 - 770 HV
Core hardness (HV_{30})	413 HV	427 HV	321 - 430 HV
Effective case depth at 550 $HV_{0.5}$ (Gear tooth)			
Outer *Ø*	0.52 mm	0.53 mm	0.45 - 0.55 mm
Flank	0.53; 0.52 mm	0.55; 0.52 mm	
Root	0.44; 0.45 mm	0.45; 0.45 mm	
Hardness at 0.1 mm depth ($HV_{0.5}$) (Gear tooth)			
Outer *Ø*	726 HV	735 HV	Information only
Flank	716; 727 HV	742; 756 HV	
Root	697; 703 HV	714; 710 HV	
Microstructure	Satisfactory	Satisfactory	Martensitic

It is evident from the hardness results that gas and oil quenching yield similar results. Core hardness values are slightly lower after gas quenching, but still well within specification.

Table 5.5. *Root-to-flank hardness ratio values for test pieces and gears.*

Sample	*Test piece case depth*	*Test piece root-to-flank hardness ratio*	*Test gear case depth*	*Test gear root-to-flank hardness ratio*	*Correlation factor for test gear*
Peak	0.50		0.52		1.02
Flank	0.48	97%	0.53	83%	1.03
Root	0.47		0.44		0.88

Table 5.6. *Hardness values measured at various locations after carburising at 920°C.*

Depth below the surface	Outer Ø *(Oil quench)*	*Flank (Oil quench)*	*Root (Oil quench)*	*Average (Oil quench)*	Outer Ø *(HPGQ)*	*Flank (HPGQ)*	*Root (HPGQ)*	*Average (HPGQ)*
Surface	762.0	762.0	762.0	762.0	760.0	760.0	760.0	760.0
0.1 mm	725.0	727.0	739.7	730.6	709.2	719.2	705.3	711.2
0.2 mm	704.9	699.4	697.1	700.5	693.5	695.5	691.3	693.4
0.3 mm	634.6	644.6	639.3	639.5	656.7	651.5	644.3	650.8
0.4 mm	566.7	554.6	562.5	561.3	567.2	578.4	587.1	577.6
0.5 mm	496.7	504.8	492.9	498.1	513.8	505.9	521.8	513.8
0.6 mm	459.4	456.3	449.3	455.0	470.0	460.4	481.8	470.7
0.7 mm	433.8	445.4	425.5	434.9	443.3	439.5	448.3	443.7
0.8 mm	429.9	424.3	413.6	422.6	426.2	425.4	418.0	423.2
0.9 mm	442.4	422.6	397.1	420.7	428.2	418.2	414.6	420.3
1.0 mm	436.6	416.2	413.8	422.2	411.8	425.3	414.7	417.3

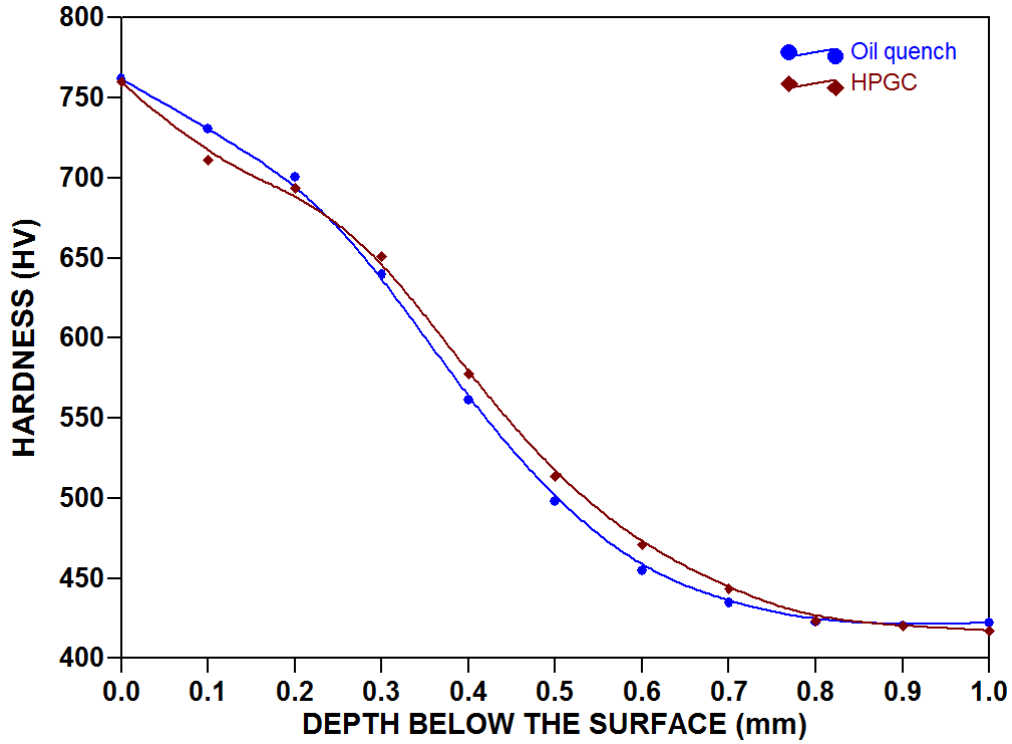

Figure 5.7. *Average hardness results after high pressure gas quenching (HPGQ) and oil quenching (carburising temperature: 920°C).*

5.5 DIMENSIONAL CHANGES AFTER CARBURISING AT 900°C

Gear manufacture requires a number of cutting and grinding sequences to shape the gear profile after carburising. Excessive distortion or dimensional change during heat treatment as a result of phase transformations and changes in surface chemistry may result in the gears requiring more machining to achieve set tolerances, possibly affecting the remaining case depth after cutting.

These dimensional changes were quantified by carburising test bars with diameters of 20 mm and 40 mm at 900°C. Any change in diameter after carburising and final heat treatment was measured and expressed as a percentage of the original diameter. The results of these tests, based on ten measurements per diameter size taken along the length of the sample, are shown in Figures 5.8 and 5.9. The maximum total dimensional change during carburising and final heat treatment was measured as 0.067 mm and 0.04 mm for the 20 mm and 40 mm diameter bars, respectively. The total dimensional changes are well below the required case depth of 0.44 to 0.55 mm, and are therefore not expected to affect the surface properties of the gears after machining to any significant extent.

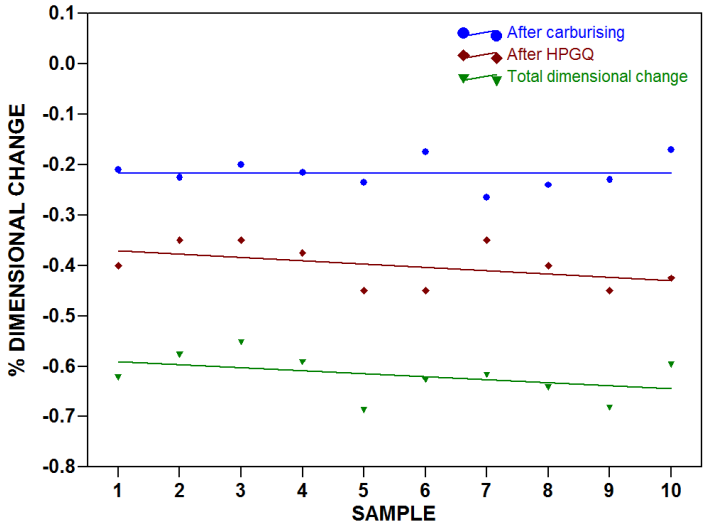

Figure 5.8. *Dimensional changes during carburising and heat treatment (bar diameter of 20 mm).*

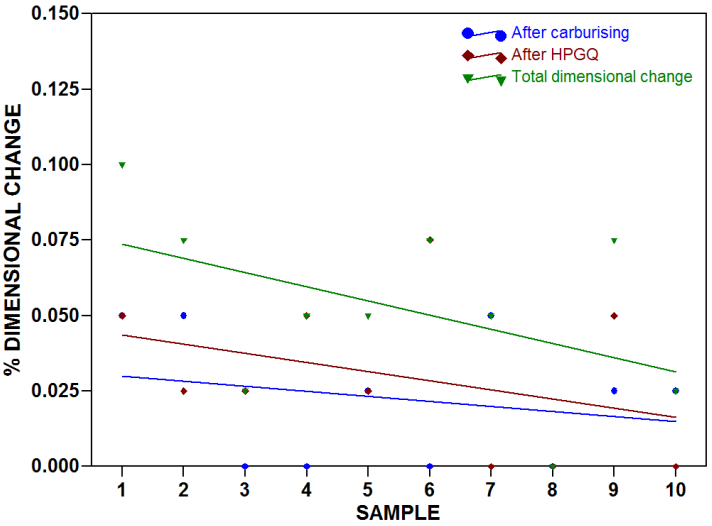

Figure 5.9. *Dimensional changes during carburising and heat treatment (bar diameter of 40 mm).*

5.6 MECHANICAL PROPERTIES AT INCREASED CARBURISING TEMPERATURES

The results described earlier suggest that increasing the carburising temperature from 900°C to 960°C, while reducing the carburising time, does not affect the carbon concentration profiles, case depths or hardness of the carburised case or core significantly. A higher carburising temperature may, however, affect the prior austenite grain size of the material, in turn affecting the tensile properties. Samples were therefore processed in accordance with the procedure described in Chapter 4 for carburising temperatures between 900°C and 960°C, and subjected to tensile testing and metallographic examination. The results of tensile tests on samples carburised at various temperatures are shown in Table 5.7.

Table 5.7. *The effect of carburising temperature on tensile properties (with the standard deviation shown in brackets).*

Temperature (°C)	*Tensile Strength (MPa)*	*Yield Strength (MPa)*	*%Elongation*
Requirement	*1180 - 1380*	*≥ 980*	*≥ 8*
900°C / Oil quench	1351 (1.7)	1079 (1.5)	14 (0.4)
900°C / Gas quench	1297 (0.7)	1037 (0.5)	16 (0.3)
920°C	1227 (0.7)	986 (0.5)	14 (0.1)
940°C	1219 (2.2)	983 (0.7)	14 (0.6)
960°C	1149 (1.3)	916 (1.2)	14 (0.3)

The tensile properties measured for a round tensile test coupon with a carburised surface depends on the nature of the carburising layer (specifically the hardness and the case depth) and the mechanical properties of the core. The properties of the carburised layer for the specific combination of the carburising temperature and time tested during this study (Table 4.6) was fairly consistent (Figure 5.5). The change in tensile properties with heat treatment condition, as noted, in Table 5.7, was therefore due to changes in the mechanical properties of the core of the tensile samples.

It is evident that all samples tested, except those carburised at 960°C, satisfied the mechanical property requirements for 16NCD13 precision gears. Although the ductility remained constant, the yield strength and ultimate tensile strength of samples carburised at 960°C did not comply with the specified requirements. In order to examine why the strength decreased with increasing carburising temperature, metallographic samples were prepared from samples carburised at 900°C to 960°C.

5.7 GRAIN SIZE AT INCREASED TEMPERATURES

The prepared samples were ground and polished. The samples were initially ground using 180 grit silicon carbide paper. The samples were then rotated at 90° to each subsequent grit size i.e. 220, 320, 400, 600, 800, 1000 and 1200, After each grinding rotation the samples were examined to ensure that no grinding marks from the previous grit size was present. The samples were then rinsed with water and alcohol to remove any grinding particles. The samples were then polished using a 9 micron and then 3 micron diamond paste. The sample was rinsed with water and alcohol after each polish. A one micron colloidal silica suspension was used to achieve the final mirror finish for the prepared micro-specimens.

A number of etching solutions exist for the determination of the of the prior austenite grain size. Each of the etchants result in surface smut requiring back polishing and re-etching. The etchants include Bechet and Beaujard's etch [52], and an etchant prepared by Lianng Zhang and Dong Cheng Guo [53]. However these etchants require etch solution temperatures i.e. 90° and 120°C respectively. An article published by A.O Benscoter and M.J Perricone [54] highlights the use of Marshall Reagent [55] which is modified using hydrofluoric acid. The etchant was successfully used on the prepared samples.

The samples were etched until a black residue appeared on the micro-specimen surface. This was removed by light back polishing ad reviewed under the microscope. This process was repeated a number of times until an acceptable microstructure was obtained. Figure 5.10 shows the microstructure for a specimen carburised at 900°C.

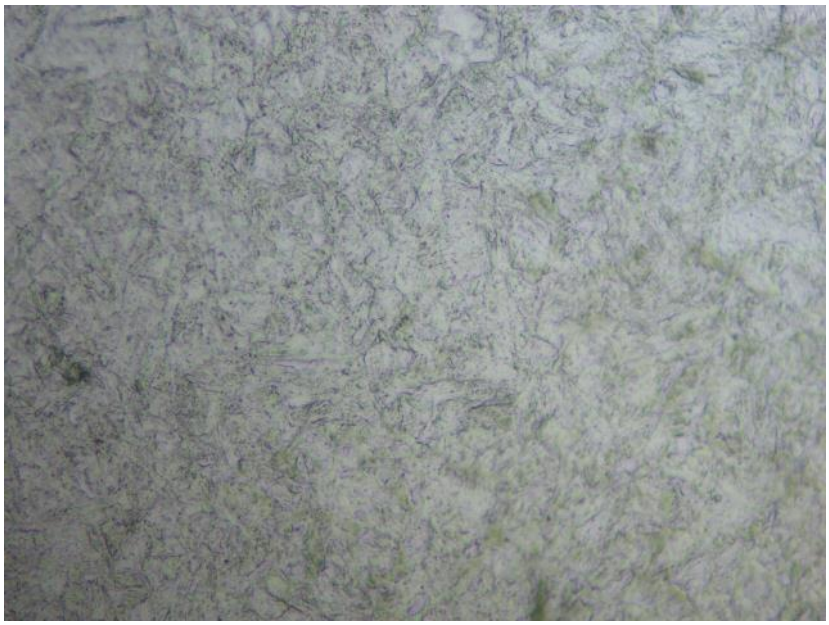

Figure 5.10. *Grain boundary austenite for a sample carburised at 900°C*

The average grain size was determined at each temperature. The results are tabulated below in Table 5.8.

Table 5.8. *Average Grain Size and ASTM Grain Size*

Temperature °C	Average Grain Size (mm)	Converted ASTM E112 Grain Size [56]
900	0,00719	10,9
920	0,00836	10,5
940	0,01000	10,0
960	0,01153	9,6

The results obtained were examined with reference to work carried out at Worcester Polytechnic Institute [56]. The results obtained, by Erik Khzouz, for a carburising AISI 8620 steel is as follows:

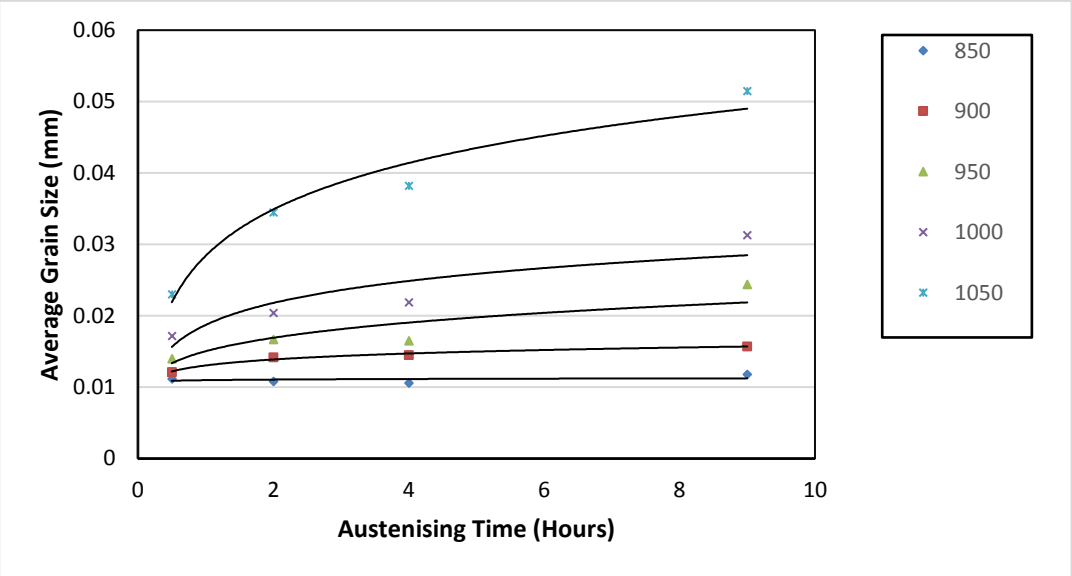

Figure 5.11. *Effect of time and temperature on grain size [56]*

The resultant data obtained as well as the results [56] would indicate that increasing the temperature, while reducing the time at the increased temperature, would not severely affect grain growth particularly in the 900 to 960°C temperature range. It is noted that above 1000°C and particularly at 1050°C there is a rapid increase in grain size for the AISI 8620 carburising steel.

5.8 CORRELATION BETWEEN MEASURED CARBON CONCENTRATION PROFILES AND THOSE PREDICTED USING DIFFUSION MODELS

Case depth, using the diffusion model calculations and Einstein's theory (2.17), were calculated. The results obtained are tabulated below.

Table 5.9. *Calculated case depth using diffusion models and Einstein's theory*

Temperature °C	Calculated Distance Fick	Calculated Distance Goldstein	Calculated Distance Collins	Calculated Distance Tibbets/Jung	Actual Distance
900	0.36	0.33	0.45	0.28	0.4990
920	0.39	0.36	0.49	0.31	0.5482
940	0.36	0.33	0.46	0.29	0.4864
960	0.34	0.30	0.43	0.27	0.4805

The graphical representation of the results is shown in Figure 5.12 below.

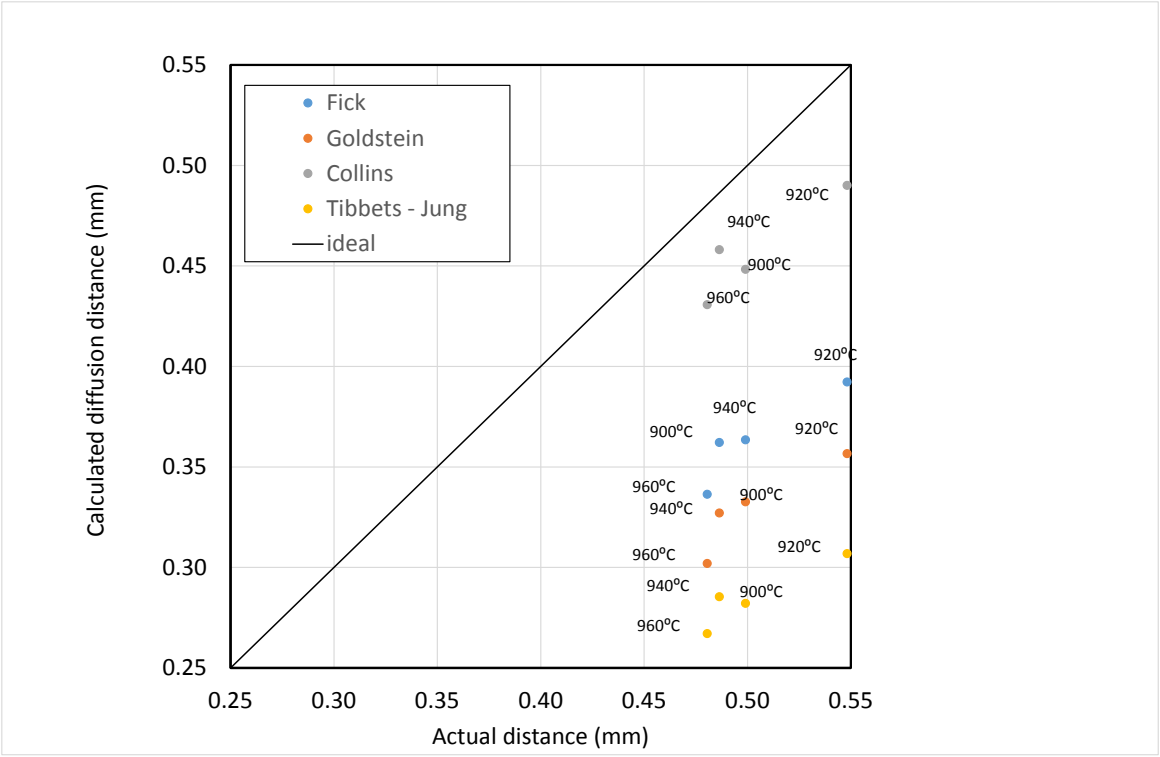

Figure 5.12. Calculated diffusion distance against actual diffusion distance

The result would indicate that Collins' model most accurately predicts the expected case depth. In order to compare the measured carbon profiles after carburising at temperatures of 900°C, 920°C, 940°C and 960°C with those obtained using the diffusion models described in Chapter 2, carbon concentration profiles were calculated based on the models proposed by Collin *et al.* [25], Goldstein and Moren [24], Tibbetts [28] and Fick [16]. The predictions of these models are compared with the actual measured carbon profiles in Figures 5.13 to 5.16.

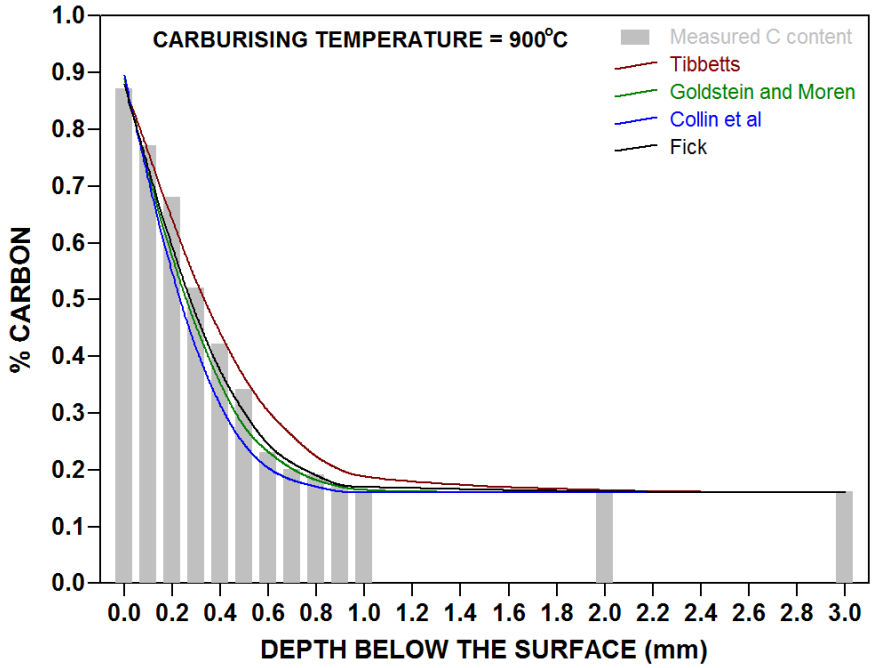

Figure 5.13. *Measured and predicted carbon concentration profiles for a carburising temperature of 900°C and a carburising time of 104 minutes.*

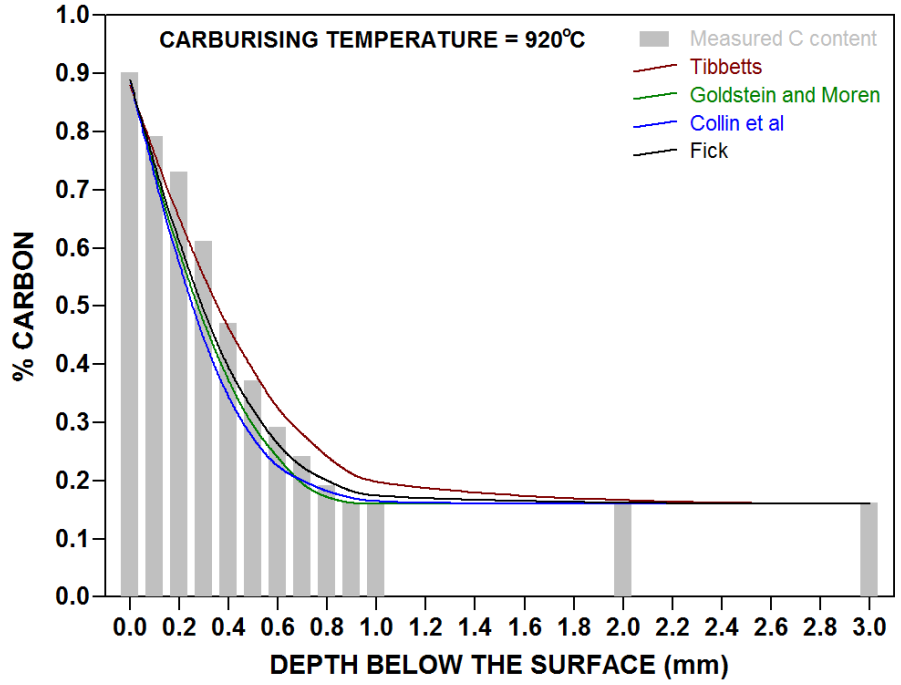

Figure 5.14. *Measured and predicted carbon concentration profiles for a carburising temperature of 920°C and a carburising time of 95 minutes.*

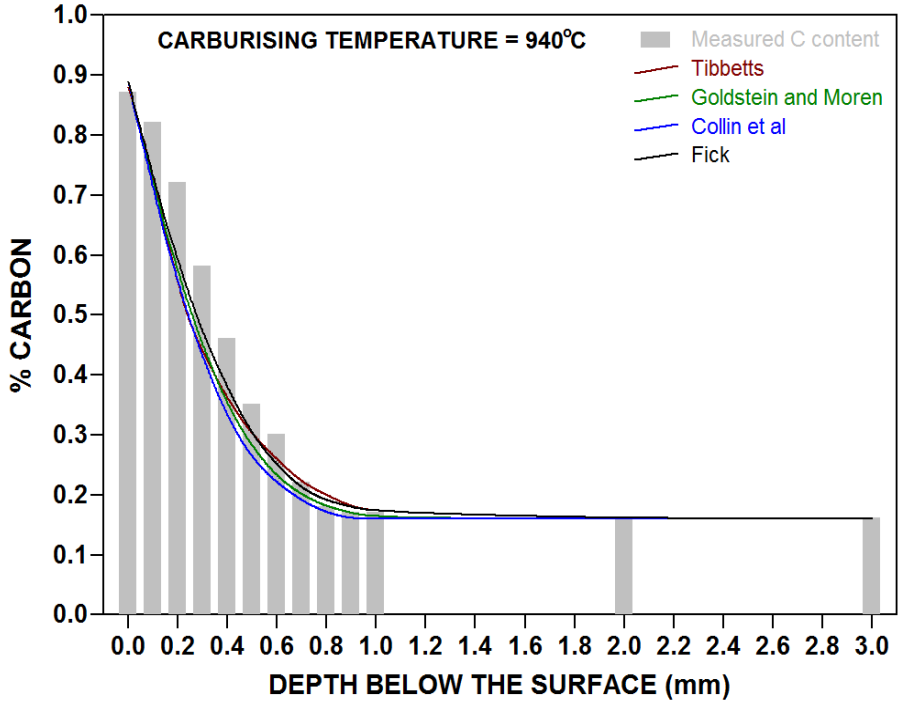

Figure 5.15. *Measured and predicted carbon concentration profiles for a carburising temperature of 940°C and a carburising time of 64 minutes.*

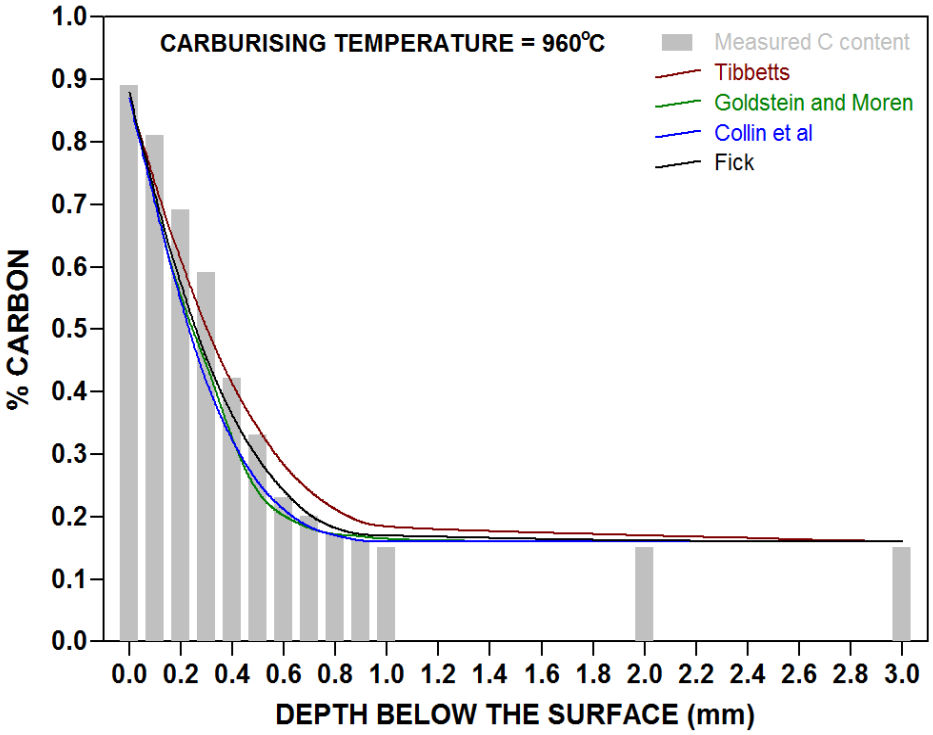

Figure 5.16. *Measured and predicted carbon concentration profiles for a carburising temperature of 960°C and a carburising time of 44 minutes.*

The results shown in Figures 5.13 to 5.16 suggest that the model proposed by Tibbett [28] and modified by Jung *et al.* [10] most accurately models the measured carbon concentration profiles. The research performed by Jung *et al.* [10] was carried out in an acetylene environment, whereas the original work by Collin *et al.* [25] was performed in an atmosphere consisting of 31.5% H_2, 23.5% N_2 and 0.6% methane (CH_4). The decomposition rate of methane (CH_4) is usually considerably lower than that of acetylene [12].

A comparative graph showing the predicted carbon value, below the surface, for each of the models, as well as the actual results obtained is shown below in Figure 5.17.

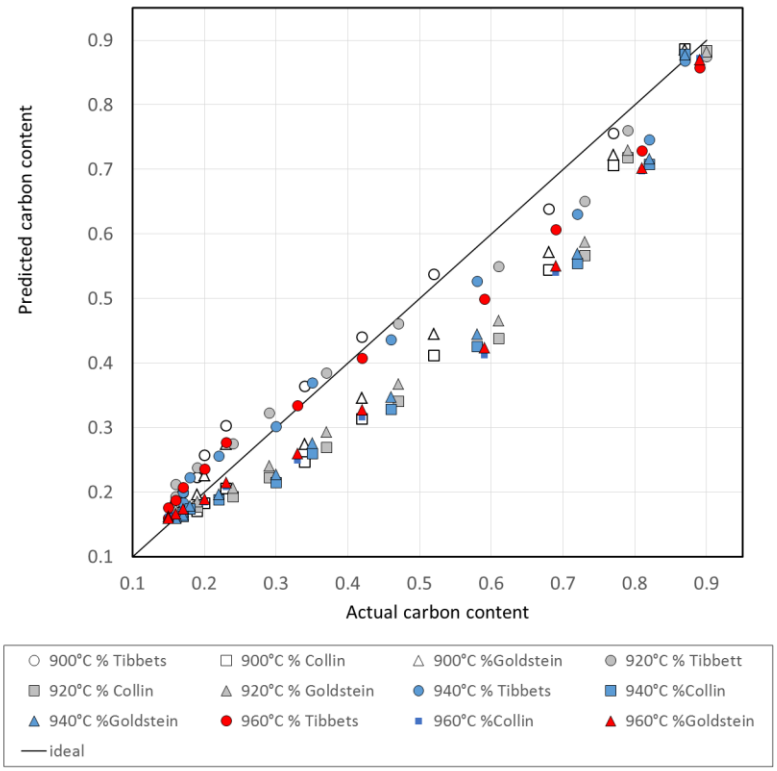

Figure 5.17. *A comparative graph based on predicted carbon (diffusivity models) versus actual carbon content based on distance from the surface.*

The graph shows that generally the calculated results predicted using the diffusivity models falls below the actual results obtained during the testing of the carburised samples. As previously noted from Figure 5.13 to 5.16, the Tibbets model was consistently the most accurate in predicting the carbon concentration at a specific position below the surface, for a specific combination of carburizing time and temperature.

5.9 MICROSTRUCTURE

The Fe-Fe_3C phase diagram shown in Figure 1.1 shows the phase transformations that occur under equilibrium conditions in binary Fe-C alloys as a function of temperature and carbon content. Conditions during gas carburising and subsequent heat treatment do not, however, approach equilibrium and kinetic diagrams are more applicable for predicting gear microstructures.

The gas carburising step during gear production is largely isothermal and an isothermal transformation (IT) diagram can be used to predict the steel microstructure during treatment. An IT diagram for 16NCD13, shown in Figure 5.18, confirms that the steel is fully austenitic at the carburising temperatures used in this investigation. The A_{c3} temperature (or the temperature on heating where the transformation from ferrite to austenite is completed) for this steel is around 780°C, and the martensite start (M_s) temperature 355°C. Above 780°C the steel should therefore be fully austenitic. Rapid quenching from the austenite phase field produces a martensitic structure with the possibility of some bainite (if the quench rate is not fast enough) and retained austenite (if the martensite finish, M_f, temperature is below room temperature). While some OEM's (Original Engine Manufacturers) in the aerospace industry insist on the use of sub-zero treatment to ensure complete transformation of austenite to

martensite, less than 5% retained austenite is usually observed in 16NCD13 after high pressure gas quenching. Sub-zero quenching therefore has limited benefit and is generally not required.

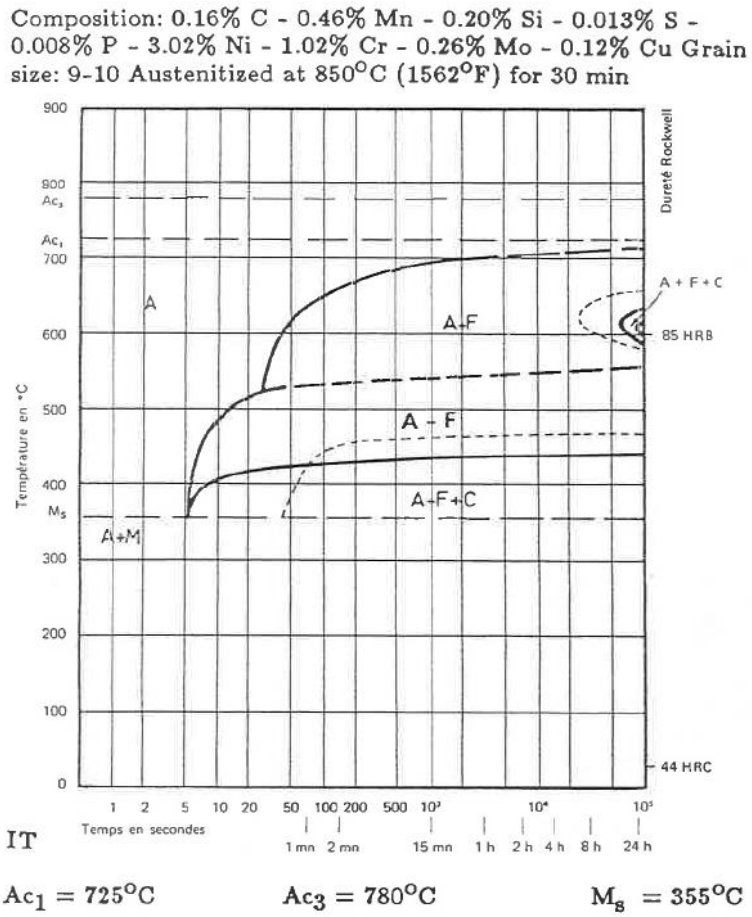

Figure 5.18. *Isothermal Transformation (IT) diagram for 16NCD13 steel [57].*

The Continuous Cooling Transformation (CCT) diagram for 16NCD13, shown in Figure 5.19, gives an indication of the expected microstructures after austenitising and quenching (high pressure gas quenching or oil quenching) from the austenite phase field. Note that this diagram is only valid for the core material after carburising, as uptake of carbon in the surface layers during the carburising treatment increases the hardenability of the surface and shifts the CCT curves to longer times.

The CCT diagram indicates that a range of hardness values can be achieved with a variation in cooling rate from the austenite phase field. Cooling from above the A_{C3} line to below 100°C in less than 40 seconds (i.e. at a cooling rate of about 1080°C per minute) produces a hardened microstructure of martensite and bainite with a hardness of approximately 44 HRC (hardness on the Rockwell scale). Conversion of this value using published hardness conversion tables [58] yields a predicted core hardness after cooling of approximately 430 HV (hardness on the Vickers scale). This hardness corresponds well with the core hardness values obtained after oil quenching in this investigation, as shown in Table 5.3. The slightly slower cooling rate of the high pressure gas quench in the furnace yields consistently lower core hardness values, suggesting a marginally higher bainite percentage in the martensitic core microstructure. The higher hardenability of the carburised case suggests that the case

microstructure should be fully martensitic after oil quenching and high pressure gas quenching. This was confirmed by the high case hardness values achieved (see Table 5.3).

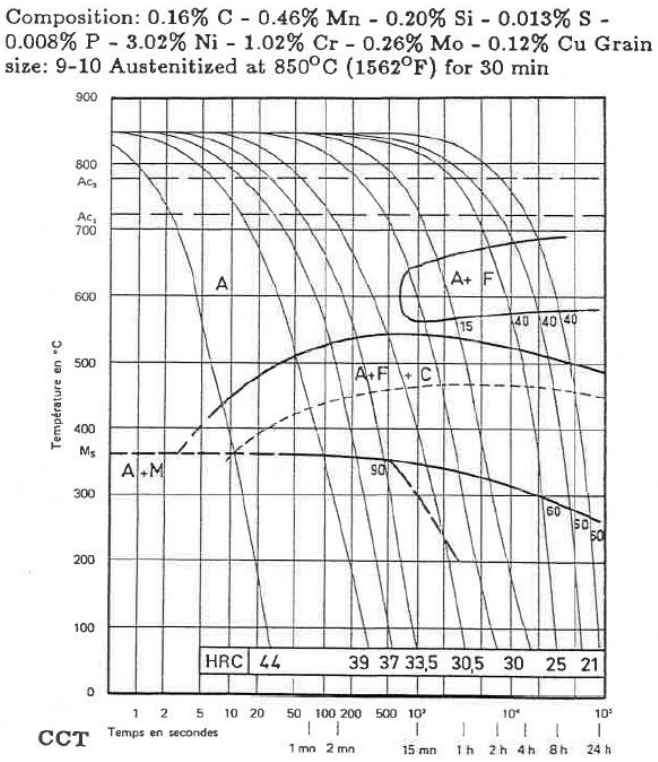

Figure 5.19. *Continuous Cooling Transformation (CCT) diagram for 16NCD13 steel [57].*

To confirm the data above and using the chemical composition of the base metal as input data (Table 4.3) Thermocalc^{TM} was used to determine the phases present, between 600° and 1000°C (Figure 5.20). The change in molar fraction of various phases with temperature is shown below.

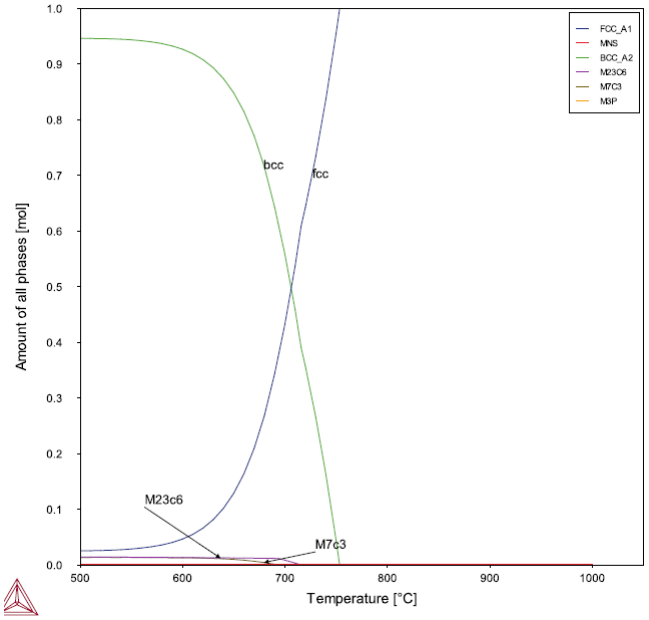

Figure 5.20. *Thermocalc^{TM}phase calulation*

From the result it would appear that all precipitates ($M_{23}C_6$, M_7C_3) have dissolved just above 700°C. This would imply that the substrate will consist purely of austenite at all carburising temperatures. The A_3 temperature is estimated at approximately 760°C.

Confirmation of the Thermocalc^{TM} prediction was carried out by sectioning the carburised samples representative test pieces and mounting the samples in resin. The metallographic samples were diamond polished to a mirror finish and etched using a 4% nital solution (No. 74 Nital in ASTM standard E407-07e1 [59]). Both core and case microstructures were examined using an optical microscope at 500x magnification.

Photomicrographs of the core and case microstructures of samples carburised at temperatures from 900°C to 960°C are shown in Figures 5.21 (a) to (h). In all the samples examined the case microstructures were observed to consist of tempered high carbon martensite, and the core microstructures of tempered low carbon martensite. Bainite was only observed in the core microstructure of the sample carburised at 960°C. It should be noted that the diagram does not consider the influence of section thickness. The samples tested during the course of this investigation were small in size and cooled rapidly on quenching. Bainite formation was therefore suppressed in all samples except those carburised at 960°C (due to the higher treatment temperature, the cooling curves would be displaced to longer times). No retained austenite was observed in the core or case microstructures, suggesting that the cooling rates achieved during high pressure gas quenching were sufficient to ensure transformation to martensite and that the martensite finish (M_f) temperature was above room temperature. The microstructures observed are consistent with the application and the hardness values measured. Significant coarsening of the microstructures with an increase in carburising temperature is not evident. Microstructural examination using an optical microscope therefore confirms that an increase in carburising temperature does not have a detrimental effect on the microstructure and properties of the core or hardened case.

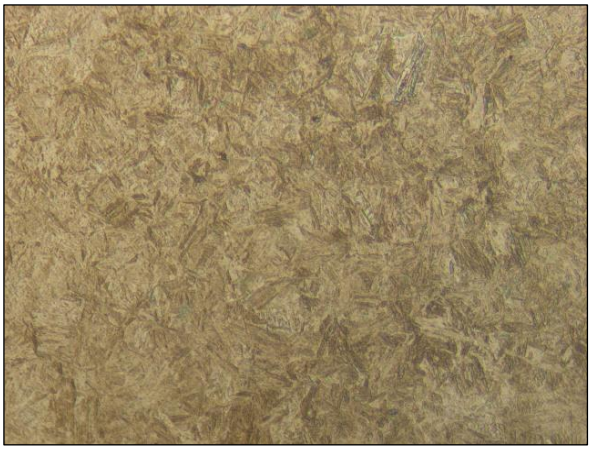

(a) Case microstructure (900°C).

(b) Core microstructure (900°C).

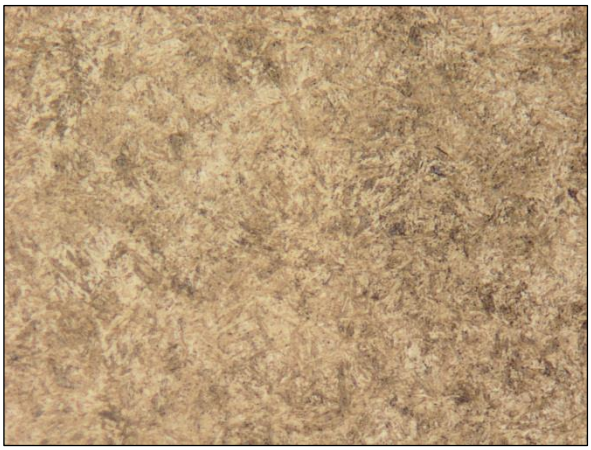

(c) Case microstructure (920°C).

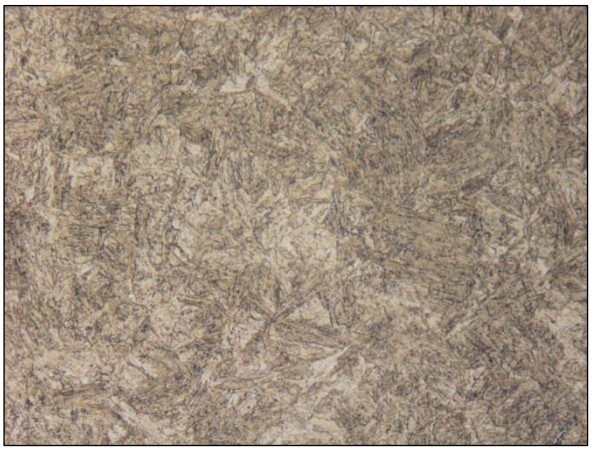

(d) Core microstructure (920°C).

(e) Case microstructure (940°C).

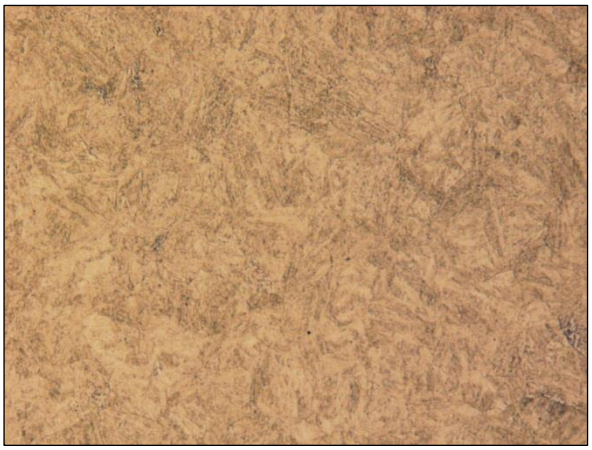

(f) Core microstructure (940°C).

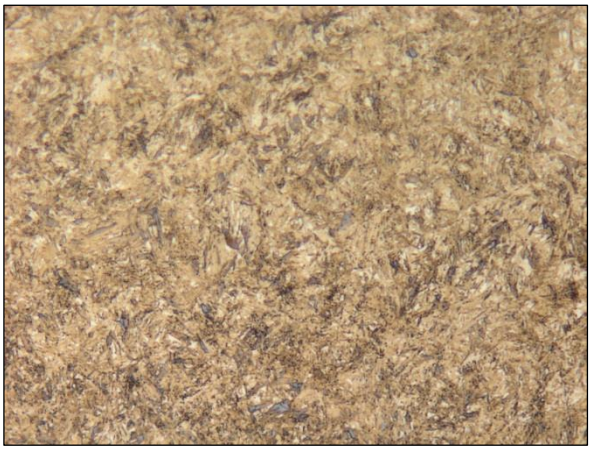

(g) Case microstructure (960°C).

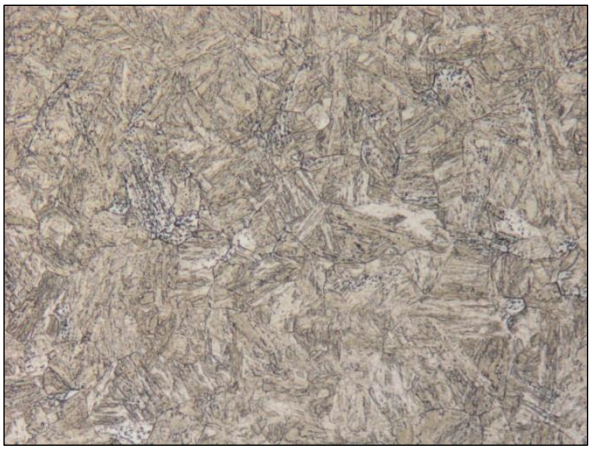

(h) Core microstructure (960°C).

Figure 5.21. *Photomicrographs of the core and case microstructures of samples carburised at temperatures between 900°C and 960°C. (Magnification: 500x).*

5.10 GAS CONSUMPTION DURING CARBURISING

Increasing the carburising temperature is likely to affect gas consumption in the furnace by increasing the carbon diffusion and reaction rates. More acetylene therefore needs to be supplied per unit time to sustain the carburising reactions. Based on the relationship

developed by Antes [43], considered in §4.6 and shown in equation (4.3), the theoretical gas flow rate, $F_{theoretical}$ can be calculated, based on the assumption that all acetylene dissociates in the furnace. The calculated total and theoretical gas flow rates are shown in Table 5.10 as a function of carburising temperature for an assumed constant carburised volume. In this table x represents the desired case depth (cm), A the total area to be carburised (cm^2), V the assumed carburised volume (cm^3), $C_{½}$ the carbon content at 50% of the desired case depth, C_{case} the carbon content at the desired case depth, C_{total} the total carbon required (in grams), F_{total} the total gas flow rate (cm^3/minute), $F_{theoretical}$ the theoretical gas flow rate (cm^3/minute), and ρ the density of the steel ($g.cm^{-3}$).

Table 5.10. *Calculated total and theoretical gas flow rates for an assumed constant carburised volume.*

Temperature	*x*	*A*	*V*	ρ	$C_{½}$	C_{case}	C_{total}	F_{total}	$F_{theoretical}$
900°C	0.05	1.0	0.05	7.87	0.620	0.37	0.00098	0.918	0.060
920°C	0.05	1.0	0.05	7.87	0.620	0.37	0.00118	1.102	0.071
940°C	0.05	1.0	0.05	7.87	0.615	0.35	0.00104	0.973	0.081
960°C	0.05	1.0	0.05	7.87	0.612	0.33	0.00111	1.036	0.115

The results shown in Table 5.10 suggest that the theoretical gas flow rate (i.e. the amount of carbon supplied during carburising, $F_{theoretical}$) increases with an increase in temperature. This can be attributed to the higher diffusion rates of carbon and the accelerated uptake of carbon during carburisation.

Table 5.11 compares the gas consumption (in normal litres per minute) in the furnace during carburising for the different carburisation temperatures, whereas the influence of increased carburising temperature on the gas consumption rate in the furnace is shown graphically in Figure 5.22. The gas consumption rate increases with an increase in temperature as more carbon is consumed per unit time during the carburisation process. This effect is, however, somewhat offset by the shorter carburisation times required at higher temperature. As shown in Table 5.2 the carburising time can be reduced significantly by increasing the carburising temperature.

Table 5.11. *The amount of gas supplied during carburisation as a function of temperature.*

Temperature (°C)	*Gas consumption (normal litres/min)*
900	34.4
920	72.4
940	80.0
960	88.2

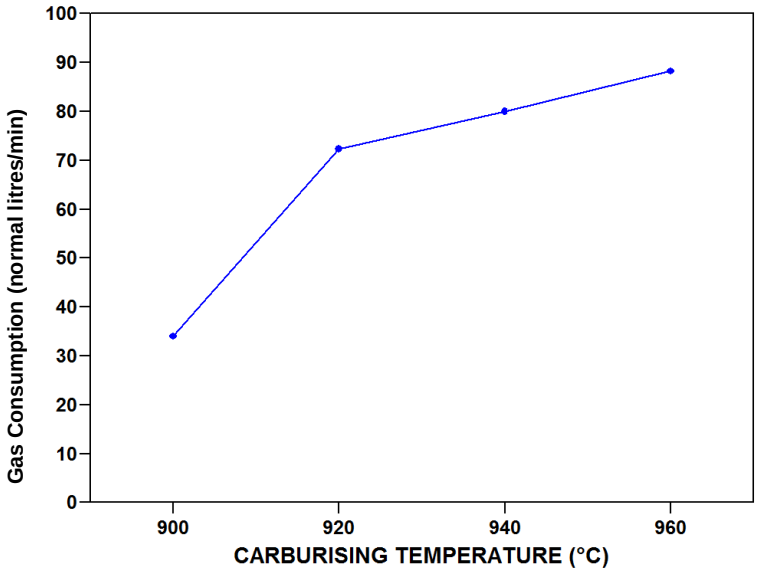

Figure 5.22. *Gas consumption in the furnace as a function of carburising temperature.*

CHAPTER 6 – CONCLUSIONS AND RECOMMENDATIONS

This investigation aimed to determine whether the total carburising time required to surface harden precision gears and shafts could be decreased by increasing the carburising temperature, without adversely affecting the specified case depth, hardness or microstructure. An industrial vacuum carburising furnace and an acetylene atmosphere were used to examine the effect of carburising temperature on the properties of the carburised surface layer in parts machined from 16NCD13 low alloy carburising steel. The following observations were made:

- **The influence of carburising temperature on the case depth and surface hardness of carburised samples:**

  Increasing the carburising temperature, while at the same time reducing the carburising time (as shown in Table 4.6), results in similar concentration profiles and case depths. Except for a marginally lower surface hardness after carburising at 900°C, no significant difference between the hardness profiles developed at different carburising temperatures was observed. Hardness measurements taken at the flank and root positions of simulated gear profiles after carburising at 920°C and 940°C were very uniform, and root-to-flank case depth ratios higher than 80% were obtained.

- **The applicability of published carbon diffusion models in austenite for predicting carbon concentration profiles during gas carburising:**

  All four carbon diffusion models evaluated during the course of this investigation approximate the measured carbon concentration profiles well. While the Collins model in conjunction with Einstein's Law most accurately predicts the case depth, the model proposed by Tibbett [28] and modified by Jung *et al.* [10] most accurately predicts the measured carbon concentration profiles. This model, which takes into account the effect of temperature, increasing carbon concentration and alloy content on the carbon diffusion coefficient in austenite, was developed for carburisation in an acetylene environment and most closely approximates the conditions used during the current investigation. It is noted that O. Karabelchtchikova [23] referenced ten diffusion models in her thesis with most of the applications assuming that carbon diffusivity either varies only with carbon concentration or is constant at fixed temperature.

- **Comparison of the experimentally measured carbon concentration profiles with carbon contents predicted by the furnace software used in commercial production:**

  This investigation confirmed that the commercial vacuum furnace Avac™ simulation software and programming cycles (based on data input into the simulation software) are capable of achieving the required case depth and hardness values after carburising. By adjusting the data input into the simulation software, the control software was able to compensate for the higher carburising temperatures by decreasing the total required carburising time. The carbon concentration profiles were predicted to a high degree of

accuracy. It should be noted, however, that the difference between the measured and simulated carbon contents increased with an increase in carburising temperature. Uniformity testing confirmed that the programming cycles and the furnace were stable and that carburising could be performed within specified requirements.

- **The influence of increasing carburising temperature on the grain size, microstructure, specimen dimensions and mechanical properties of the vacuum remelted low carbon carburising steel used in the commercial production of precision gears:**

  After final heat treatment, the carburised case microstructures were observed to consist of tempered high carbon martensite, and the core microstructures predominantly of tempered low carbon martensite. Bainite formation was suppressed in all samples except those carburised at 960°C. No retained austenite was observed in the core or case microstructures, and the measured hardness values were well within specification for the application. The prior austenite grain size was marginally coarser after carburisation at 960°C than at 900°C. The slightly coarser grain equates to an ASTM Grain Size variation of 1. This change is not considered significant. All samples tested, except those carburised at 960°C, satisfied the mechanical property requirements for 16NCD13 precision gears. Although the ductility remained sufficiently high, the yield strength and ultimate tensile strength of samples carburised at 960°C did not comply with the specified requirements. The observed changes in the dimensions of samples carburised at 900°C were minimal and not expected to affect the surface properties of the gears after machining to any significant extent. It is recommended, however, that the dimensional variations at higher carburising temperatures be ascertained as part of a future study. The high pressure gas quench used during commercial production was shown to be capable of producing the desired case depths and hardness values. The presence of bainite in the core samples carburised at 960°C are not clear but are considered beyond the scope of the current study.

The results of this investigation suggest that the current carburising system used at Turbomeca Africa for surface hardening of precision gears and shafts is capable of achieving the required case and core properties at carburising temperatures up to 940°C. Such an increase in carburising temperature results in a significant reduction in the required total carburising time. Prior to the introduction of higher carburising temperatures for commercial production, however, the limitations of the furnace system should be considered. The current Ipsen Avac 524™ furnace used in production is 17 years old and limited to a 10 bar quench pressure. Furnaces currently available on the market are capable of quench pressures up to 20 bar. Other furnace technologies commercialised in recent years include dynamic quenching and reversing gas flow [60]. The dynamic quenching process consists of three steps. During the first stage a high quenching severity is maintained until a pre-programmed temperature is reached. In the second step the quenching severity is reduced for a specified time to allow temperature equalisation in the part. The final step sees an increased quench severity until the end of the quench process. Modern gas quenching chambers now also offer the possibility of reversing the gas flow direction during quenching. The flow of gas is alternated back and forth in the furnace,

reducing the difference in cooling rate of parts placed in different layers in the furnace. This reduces the spread of distortion in the furnace load [60].

The type of gas used during high pressure gas quenching may also need to be assessed from a cost saving point of view. Hydrogen has a heat transfer coefficient almost three times that of nitrogen and can achieve quenching speeds similar to oil [49]. This may be of importance in applications where higher temperatures are used or larger diameter stock is carburised.

REFERENCES

[1] S.H. Avner. *Introduction to physical metallurgy.* 2nd edition. McGraw-Hill, Singapore.1974. pp. 317-326.

[2] Substances and Technologies (Substech), *http://www.substech.com/dokuwiki/doku.php?id=iron-carbon_phase_diagram.* Accessed in March 2015.

[3] The Welding Institute (TWI), *http://www.twi-global.com/technical-knowledge/faqs/process-faqs/faq-what-is-carburising-carbonitriding/.* Accessed in March 2015.

[4] Mechanical Technology (MechTech), *http://4mechtech.blogspot.com.au/2013/11/ case-hardening-process-pack-carburizing.html.* Accessed in March 2015.

[5] K.-E. Thelning. *Steel and its heat treatment.* Butterworths, London. 1975. pp. 358.

[6] M. Jaster. *Why vacuum carburizing? Heat treatment alternative offers advantages over conventional methods*. Gear Technology, March/April 2010. pp. 31-35.

[7] S. Bruce, V. Cheetham and P.F. Stratton. *Low-pressure carburising systems: A review of current technology*. *http://www.edwardsvacuum.com/asia/newsletters/vacasia/0709/pdf/Low_Pressure_Systems.pdf.* Accessed in March 2015.

[8] M. Sugiyama, K. Ishikawa and H. Iwata. *Using acetylene for superior performance vacuum carburizing.* Proceedings of the 18th ASM Conference on Heat Treating, held in Cincinatti, OH, from 12-15 October 1998. 1998. pp. 49-56.

[9] M. Qin. *Vacuum carburising and high pressure gas quenching technology in automotive industry.* International Heat Treatment and Surface Engineering, vol. 2, no. 3/4. 2008. pp. 116-120.

[10] M. Jung, S. Oh, Y.-K. Lee. *Predictive model for the carbon concentration profile of vacuum carburized steels with acetylene.* Metals and Materials International, vol. 15, vol. 6. 2009. pp. 971-975.

[11] L.-D. Liu and F.-S. Chen. *The influences of alloy elements on the carburized layer in steels using vacuum carburization in an acetylene atmosphere*. Materials Chemistry and Physics, vol. 82. 2003. pp. 288-294.

[12] M. Sugiyama. *Vacuum carburizing.* Journal of the Japan Society for Heat Treatment, vol. 37, no. 3. 1998. pp. 154.

[13] N. Okumura and A. Iwase. *Vacuum carburizing using acetylene gas.* Journal of the Japan Society for Heat Treatment, vol. 38, no. 4. 1998. pp. 195.

[14] W. Gräfen and B. Edenhofer. *Acetylene low-pressure carburising - A novel and superior carburising technology*. Heat Treatment of Metals, vol. 26, no. 4. 1999. pp. 79-83.

[15] P.A. Thornton. *Fundamentals of engineering materials.* Prentice-Hall, Englewood Cliffs. 1985.

[16] A. Fick. *On Liquid Diffusion.* The London, Edinburgh and Dublin Philosophical Magazine and Journal of Science, vol. X. 1855. pp. 30-39. (Abstracted by the author from the German original: *Űber Diffusion*. Annalen der Physik und Chemie, vol. 94. 1855. pp. 59-86).

[17] T.Lovett,*http://www.learneasy.info/MDME/focus/materials/enmat/LECTURES/Lecture-06/images/*. Accessed in March 2015.

[18] University of Western Ontario, *www.physics.uwo.ca*, *Chapter 5: Diffusion,* pp.1-9. Accessed in March 2015.

[19] E.A. Brandes and G.B. Brook (eds.). *Smithells Metals Reference Book*. 7th edition, Butterworth-Heinemann, Oxford, 1992.

[20] W.D. Callister and G.D. Rethwisch. *Materials Science and Engineering: An introduction.* 8th Edition. John Wiley & Sons, Hoboken, NJ. 2010.

[21] National Bureau of Standards. *Tables of the error function and its derivative*. Applied Mathermatics Series, vol. 41. Washington DC. 1954.

[22] C. Wells and R. F. Mehl. *Rate of diffusion of carbon in austenite in plain carbon, in nickel, and in manganese steels*. Chemical Abstracts, vol. 34. 1940. p. 7241.

[23] O. Karabelchtchikova. *Fundamentals of mass transfer in gas carburising*. PhD Thesis, Worcester Polytechnic Institute. Worcester, MA. 2007.

[24] J.I. Goldstein and A.E. Moren. *Diffusion modelling of the carburisation process*. *Metallurgical and Materials Transactions A, vol.* 9A, no. 11. 1978. pp. 1515-1525.

[25] R. Collin, S.Gunnarson and D. Thulin. *A mathematical model for predicting carbon concentration profiles of gas-carburized steel.* Journal of the Iron and Steel Institute, October 1972. pp. 785-789.

[26] T. Wada, H. Wada, J.F Elliot, J. Chipman. *Activity of carbon and solubility of carbides in the FCC Fe-Mo-C, Fe-Cr-C, and Fe-V-C alloys.* Metallurgical Transactions, vol. 3, no. 11. 1972. pp. 2865-2872.

[27] F. Neumann and B. Person. *Beitrag zur metallurgie der gasaufkohlung - Zusammenhang zwischen dem C-potential der gasphase und des werkstückes unter berücksichtigung der legierungselemente.* Härterei-Technische Mitteilung, vol. 23, no. 4. 1968. pp. 296-308.

[28] G.G. Tibbetts*. Diffusivity of carbon in iron and steels at high temperatures.* Journal of Applied Physics, vol. 51, no. 9. 1980. pp. 4813-4816

[29] K.E Thelning. *Steel and its Heat Treatment*. Butterworths, London. 1975. pp. 24.

[30] G.E. Totten, K. Funatani and L. Xie (eds.). *Handbook of Metallurgical Process Design.* Marcel Dekker, Inc., New York, NY. 2004.

[31] A.G. Guy and J.J. Wren. *Elements of Physical Metallurgy*. 2nd Edition. Addison-Wesley, Reading, MA. 1973.

[32] P.G. Shewmon. *Transformations in metals.* McGraw-Hill, New York, NY. 1969.

[33] E.O. Hall and N.J. Petch. *The cleavage strength of crystals.* Journal of the Iron and Steel Institute, vol. 174. 1953. pp. 25-28.

[34] E. Khzouz. *Grain growth kinetics in steels.* BSc Project Report, Worcester Polytechnic Institute. Worcester, MA. 2011. Pp. 5-6

[35] C. Yue, L. Zhang, S. Liao and H. Gao. *Kinetic analysis of the austenite grain growth in GCr15 Steel.* Journal of Materials Engineering and Performance, vol. 19, no. 1. 2009. pp. 112-115.

[36] S. Illescas, J. Fernandez and J.M. Guilemany. *Kinetic analysis of the austenitic grain growth in HSLA steel with a low carbon content.* Materials Letters, vol. 62. 2008. pp. 3478-3480.

[37] A. Giumelli. *Austenite grain growth kinetics and the grain size distribution.* M.A.Sc. Thesis, University of British Columbia. Vancouver, Canada. 1995.

[38] R. Stringfellow. *Prediction and control of heat treat distortion of helicopter gears.* Report prepared for the Aviation Applied Technology Directorate, U.S. Army Aviation Troop Command (Report number: USAATCOM TR 95-D-5). August 1995.

[39] Latrobe Specialty Steel Company. *Lescalloy® 16NCD13 Var-Arc® Data Sheet.* 2007.

[40] ASTM A370-14. *Standard test methods and definitions for mechanical testing of steel products.* ASTM International, West Conshohocken, PA. 2014.

[41] SAE AMS 2750E. *Pyrometry.* SAE International, Warrendale, PA. 2012.

[42] D.S. Clark and W.R. Varney. *Physical Metallurgy for Engineers*. Van Nostrand, Princeton, NJ. 1962. p. 204.

[43] Ipsen USA, http://*www.Ipsenusa.com/documents/Ipsen-USA/Editorial/Avac-Brochure .pdf.* Accessed in May 2015.

[44] H.W. Antes. *Calculating the gas flow rate for vacuum carburization*. Heat Treating Progress. August 2005. pp. 51-53.

[45] V. Hauer, K. Loser, D.R Faron and D. Bottom. *Low-distortion heat treatment of transmission components,* Gear Technology, October 2011. p. 88.

[46] ALD Vacuum Technologies, *www.ald-vt.com/cms/en/vacuum-technology/ technologiesvacuum-heat-treatment/vacuum-case-hardening/high-pressure-gas-quenching/.* Accessed March 2015.

[47] B.L. Ferguson, Z. Li and A.M. Freborg. *Simulation of gas quenching of steel parts.* Thermal Processing. 2013. p 54-60.

[48] J. Kowalewski, M. Korecki and J. Olejnik. *Next-generation HPQ vacuum furnace.* Heat Treating Progress, September 2008. pp. 39-44.

[49] BOC (The Linde Group), *www.boconline.co.uk/internet.lg.lg.gbr/en/images/Principles %20of%20Quenching%20and%20Cooling410_114391.pdf*. Accessed May 2015.

[50] M. Lohrmann and W. Gräfen. *Advanced Process and Furnace Technology for Case hardening using Low Pressure and Plasma Carburising combined with Gas Quenching.* ASM Heat Treating Conference, 9-12 October 2000.

[51] F.J. Otto and D.H. Herring. *Improvements in dimensional control of heat treated gears*. Gear Solutions, June 2008. p. 22-29.

[52] G.F Vander Voort. *Revealing Prior-Austenite Grain Boundaries in Heat treated Steels.* Industrial Heating, Vol 78. April 2010. Pp. 48-52.

[53] Lianng Zhang and Dong Cheng Guo. *A General Etchant for Revealing Prior-Austenite Grain Boundaries in Steel.* Materials Characterization 30. 1993. Pp 299-305. [53

[54] A.O Benscoter and M.J Perricone. *Origins, Modifications and New Applications.* Microscope Microanal 11 (Suppl 2), 2005, pp. 76-78.

[55] Marshall W.A. *A Non-Electrolytic Smoothing Treatment for Steel.* Electrodepositor's Tech Soc, 1952, 28:p 27-46.

[56] E. Khzouz. *Grain Growth Kinetics in Steels.* BSc Project Report, Worcester Polytechnic Institute. Worcester, MA. 2011. pp. 42.

[57] G.F. Vander Voort. *Atlas of Time-Temperature Diagrams for Iron and Steel.* ASM International, Materials Park, OH. 1991. p. 193.

[58] ASTM E112-13. *Standard test methods for determining average grain size.* ASTM International, West Conshohocken, PA. 2013.

[59] ASTM E407-07e1. *Standard practice for microetching metals and alloys.* ASTM International, West Conshohocken, PA. 2007.

[60] V. Hauer, D. Bolton, M. Lifshits and K. Löser. *Application of "Dynamic quenching" and "Reversing gas flow" technologies to minimize distortion values after high pressure gas quenching*. *http://web.ald-vt.de/cms/fileadmin/pdf/presse/ Dynamic_ quenching_and_Reversing_gas_ flow.pdf.* Accessed May 2015.